Thesis for Doctor of Philosophy
in Natural Science with a
specialization in Chemistry

Development of automated nanopore-based biosensor platform:

ATCUN-peptide functionalization enables highly sensitive detection of Cu(II) ions in fluids

Shitanshu Devrani

Department of Chemistry and Molecular Biology

Gothenburg, 2025

Doctoral Dissertation in Natural Science with a specialization in Chemistry
Department of Chemistry and Molecular Biology
University of Gothenburg

Printed by Kompendiet AB, Gothenburg, Sweden, 2025
ISBN: 978-91-8115-455-9 (PRINT)
ISBN: 978-91-8115-456-6 (PDF)
Available online at http://hdl.handle.net/2077/89606

Dedicated to the
undying spirit to go all the way

What Matters Most is How Well You Walk Through the Fire, 1999
Charles Bukowski

"If you're going to try, go all the way. Otherwise, don't even start. This could mean not eating for three or four days. It could mean freezing on a park bench. It could mean jail. It could mean derision. It could mean mockery--isolation. Isolation is the gift. All the others are a test of your endurance, of how much you really want to do it. And, you'll do it, despite rejection and the worst odds. And it will be better than anything else you can imagine. If you're going to try, go all the way. There is no other feeling like that. You will be alone with the gods, and the nights will flame with fire. You will ride life straight to perfect laughter. It's the only good fight there is."

Abstract

Copper is essential for energy production, antioxidant defense, and neurotransmitter synthesis; its dysregulation is implicated in disorders such as Wilson's, Menkes, and Alzheimer's disease. This thesis addresses the need for sensitive, rapid copper(II) detection to improve clinical monitoring and diagnosis.

The thesis focuses on the development of an automated nanopore-based biosensor platform for copper(II) detection to address the clinical need for rapid and accurate copper monitoring. The results of this thesis are summarized in three papers.

Paper I reports the development of an efficient synthetic protocol to the fluorescently labelled Amino-Terminal Cu(II) and Ni(II) binding (ATCUN) peptides. Various coupling conditions are investigated and improved coupling protocols significantly increase yields. Physico-chemical properties of the rhodamine-labelled ATCUN peptide were investigated, resulting in optimized quenching and binding efficiencies at pH 6.5.

Paper II describes about platform with multiplexed voltage-to-current (IV) and fluorescence measurements of the samples. This automated platform was called Bio-Sensei, which incorporates a robotic pipetting arm, picoampermeter and fluorescence measurement diode. This platform enables measurement, collection of data from instruments and storage of the data. The platform is tested with ATCUN functionalized nanopore membranes in Cu(II) spiked MES/KCL buffer at pH 6.5. Results show the ability to detect Cu(II) up to femtomolar concentrations in buffer.

Paper III presents the integration of reconfigurable microfluidics with the automated platform, and measurements in human serum mimics samples, by spiking them with Cu(II). This is followed by data analysis using neural network algorithms to predict Cu(II) concentrations in the solution. Results of this study show that nanopores functionalized with rhodamine labelled ATCUN peptide showed improved sensitivity to Cu(II) ions than previously used FAM labelled ATCUN.

The results of this thesis contribute to the development of the platform with the potential to enable the measurement of Cu(II) in clinical samples, such as Wilson's disease diagnosis or monitoring. Future directions include expansion to other metal ions, integration

with wearable technology, and further refinement of machine learning algorithms to enhance clinical utility.

Sammanfattning

Avhandlingen fokuserar på utvecklingen av en automatiserad nanoporöbaserad biosensorplattform för koppar(II)-detektion för att adressera det kliniska behovet av snabb och noggrann kopparövervakning. Resultaten från denna avhandling sammanfattas i tre artiklar.

Artikel I redovisar utvecklingen av ett effektivt syntetiskt protokoll för fluorescensmärkta Amino-Terminala Cu(II) och Ni(II) bindande (ATCUN) peptider. Olika kopplingsförhållanden undersöks och förbättrade kopplingsprotokoll ökar signifikant utbytena. Fysikalisk-kemiska egenskaper hos rhodaminmärkta ATCUN-peptider undersöktes, vilket resulterade i optimerad släcknings- och bindningseffektivitet vid pH 6.5.

Artikel II beskriver en plattform med multiplexade spänning-till-ström (IV) och fluorescensmätningar av proverna. Denna automatiserade plattform kallades Bio-Sensei, vilken inkorporerar en robotisk pipetteringsarm, pikoamperemeter och fluorescensmätningsdiod. Denna plattform möjliggör mätning, datainsamling från instrument och datalagring. Plattformen testades med ATCUN-funktionaliserade nanoporimembran i Cu(II)-spikade MES/KCl-buffrar vid pH 6.5. Resultaten visar förmågan att detektera Cu(II) upp till femtomolära koncentrationer i buffert.

Artikel III presenterar integrationen av rekonfigurerbar mikrofluidik med den automatiserade plattformen, och mätningar i humana serumimitatprover genom spikining med Cu(II). Detta följdes av dataanalys med neurala nätverksalgoritmer för att prediktera Cu(II)-koncentrationer i lösningen. Resultaten från denna studie visar att nanoporer funktionaliserade med rhodaminmärkta ATCUN-peptider uppvisade förbättrad känslighet för Cu(II)-joner jämfört med tidigare använda FAM-märkta ATCUN.

Resultaten från denna avhandling bidrar till utvecklingen av plattformen med potential att möjliggöra mätning av Cu(II) i kliniska prover, såsom för diagnos eller övervakning av Wilsons sjukdom. Framtida riktningar inkluderar expansion till andra metalljoner, integrering med bärbar teknik, och vidare förfining av maskininlärningsalgoritmer för att förhöja klinisk nytta.

Contents

Abbreviations

4PL	Four-Parameter Logistic
5PL	Five-Parameter Logistic
Al_2O_3	Aluminum Oxide
ATCUN	Amino-Terminal Cu(II) and Ni(II) binding
AUC	Area Under the Curve
BFGS	Broyden–Fletcher–Goldfarb–Shanno
BODIPY-FL	4,4-Difluoro-4-bora-3a,4a-diaza-s-indacene propanoic acid
CAGR	Compound Annual Growth Rate
CLSM	Confocal Laser Scanning Microscopy
CNC	Computer Numerical Control
Cu(II)	Copper(II) ion
Dap	Diaminopropionic acid
DNA	Deoxyribonucleic Acid
EDC	1-Ethyl-3-(3-dimethylaminopropyl) carbodiimide
EDL	Electric Double Layer
ETL	Extract Transform Load
FAM	5(6)-Carboxyfluorescein
fg	Femtogram
Fmoc	Fluorenylmethyloxycarbonyl
Gly	Glycine
G6PD	Glucose-6-Phosphate Dehydrogenase
HATU	Hexafluorophosphate Azabenzotriazole Tetramethyl Uronium
HBTU	Hexafluorophosphate Benzotriazole Tetramethyl Uronium
His	Histidine
HPLC	High-Performance Liquid Chromatography
IoT	Internet of Things
I-V	Current-Voltage
IV	Current-Voltage (interchangeable with I-V)
kPa	Kilopascal
KCL	Potassium Chloride
LFAs	Lateral Flow Assays
LOD	Limit of Detection
M	Molar (concentration)
MES	2-(N-morpholino)ethanesulfonic acid
m-ADBio	Modified Artificial Dynamic Biosystem

mL	Milliliter
MLP	Multilayer Perceptron
MoS_2	Molybdenum Disulfide
MOFs	Metal-Organic Frameworks
nS	Nanosiemens
Ni(II)	Nickel(II) ion
NIR	Near-infrared Radiation
nm	Nanometer
PCA	Principal Component Analysis
PET	Poly(ethylene terephthalate)
PFP	Pentafluorophenol
PNA	Peptide Nucleic Acid
PMMA	Poly(methyl methacrylate)
POC	Point-of-Care
PVD	Physical Vapor Deposition
PyBOP	Benzotriazol-1-yloxytripyrrolidinophosphonium hexafluorophosphate
RhoB	Rhodamine B
ROC	Receiver Operating Characteristic
ROAUC	Receiver Operating Characteristic Area Under the Curve
RT-qPCR	Reverse Transcription Quantitative Polymerase Chain Reaction
Sar	Sarcosine
SARS-CoV-2	Severe Acute Respiratory Syndrome Coronavirus 2
SEIR	Susceptible-Exposed-Infectious-Recovered
SPPS	Solid-Phase Peptide Synthesis
UV/Vis	Ultraviolet-Visible
Xaa	Any amino acid
β-Ala	Beta-Alanine
µL	Microliter
µm	Micrometer

Publications

The dissertation is based on the following research papers, which are referred to in the text by their Roman numerals.

- **Paper I**: Hintzen‡, J.C.J; Devrani, S‡.; Carrod, A.J.; Bayik, M.B.; Tietze, D.; Tietze, A.A. Fluorescence Labeling of Peptides: Finding the Optimal Protocol for Coupling Various Dyes to ATCUN-like Structures (2024), ACS Org. Inorg. Au. (4), 5 (Published) https://doi.org/10.1021/acsorginorgau.4c00030
  ‡ Equal contribution

- **Paper II**: Devrani, S.; Tietze, D.; Tietze, A. A., Automated Microfluidic Platform for High-Throughput Biosensor Development. 2025, (3), 4 2400116. (Published) https://doi.org/10.1002/adsr.202400116

- **Paper III**: Devrani, S.; Hintzen, J.C.J.; Nasiri, R.; Tietze, D.; Unksov, I.; Lapins, N.; Herland, A; Tietze, A, Multimodal Microfluidic Biosensor with Neural Network Analytics for Accurate Detection of Cu(II) in Human Serum (Manuscript Draft)

- **Paper I:** data curation, formal analysis, investigation, validation, visualization, writing-original draft

- **Paper II:** conceptualization, data curation, formal analysis, investigation, validation, methodology, visualization, writing-original draft, writing-review & editing

- **Paper III:** conceptualization, data curation, formal analysis, investigation, validation, methodology, visualization, writing-original draft, writing-review & editing

Chapter 1

1.0 Introduction

Numerous biological processes rely on copper homeostasis for proper functioning. This includes energy production, antioxidant defense, and neurotransmitter synthesis.[1] Dysregulation of copper levels can lead to severe health issues, such as Menkes disease;[2, 3] Wilson's disease,[4] and neurodegenerative conditions like Alzheimer's disease.[3, 5] Accurate detection of copper ions in human serum is essential for early diagnosis, treatment monitoring, and understanding the pathophysiology of copper-related disorders.[2, 3]

Recent advances in biosensor technology significantly improve our ability to detect and quantify copper ions in biological samples. Several approaches emerge, among them enzyme-based biosensors have shown high sensitivity and selectivity for various analytes, including pesticides and heavy metals.[6] These biosensors often exploit the inhibition of specific enzymes by copper ions, providing a "physiologically relevant" method of detection. Nanomaterials have also played a crucial role in enhancing biosensor performance. For instance, Cu-MOFs (Metal-Organic Frameworks) nanoparticles with sizes from 7 to 19 nm have been used as biosensors for triiodothyronine hormone (T3) detection, while HKUST-1 (a specific type of Cu-MOF) composites with glucose oxidase have been utilized for glucose biosensing.[7,8] These materials offer unique properties such as high surface area, tunable pore size, and excellent biocompatibility, making them ideal candidates for biosensor development.[7] Near-infrared (NIR) persistent luminescent nanoparticles emerge as powerful tools in the realm of optical sensing for biosensing and bioimaging in cancer analysis.[9, 10] While not specifically designed for copper detection, these advancements in NIR technology could potentially be adapted for metal-ion sensing, offering improved tissue penetration and reduced background interference.[9] However, existing technologies

often struggle to combine the sensitivity, selectivity, and robustness required for clinical copper detection, particularly in complex biological matrices like human serum, where interferents and dynamic physiological conditions pose significant challenges.

Furthermore, the development of microfluidic platforms have revolutionized biosensor design and testing.[11] These systems allow for high-throughput screening, rapid optimization, and integration of multiple sensing modalities. The combination of microfluidics with electrochemical and fluorescence-based detection methods has proven particularly effective for metal-ion sensing.[11] In the context of clinical applications, there is growing interest in developing point-of-care devices for rapid and accurate copper detection.[12]

This thesis aims to develop and validate an automated, nanopore-based biosensor platform for highly sensitive and selective detection of Cu(II) ions in biological fluids, with a view toward clinical application in disorders such as Wilson’s disease.

Chapter 2

2.0 Background

2.1 Potential of biosensors

The biosensor field is rapidly expanding due to rising demand for early chronic disease diagnosis, point-of-care testing, and sustainable healthcare solutions. Driven by technological advancements as shown in Figure 1, the global biosensor market is projected to grow from $27 billion in recent years to $62 billion by 2032, reflecting a compound annual growth rate (CAGR) of 8.8%.[13-17]

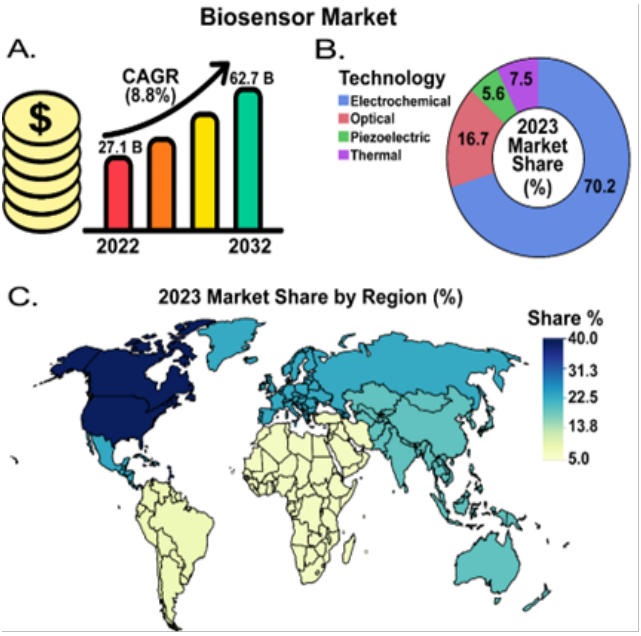

Figure 1: (A) Market Growth: The biosensor market is projected to grow from $27.1 billion in 2022 to $62.7 billion by 2032, with a compound annual growth rate (CAGR) of 8.8%. (B) Technology Market Share (2023): Electrochemical: 70.2%, Optical: 16.7%, Piezoelectric: 5.6%, Thermal: 7.5%. (C) Regional Market Share (2023): The map illustrates the distribution of market share globally, with darker regions indicating higher market share percentages, reaching up to 40%.

North America dominates regional demand, driven by advanced healthcare infrastructure, with the medical sector accounting for over 60% of applications, particularly in point-of-care diagnostics.[14, 18] Specifically, the United States market is projected to experience

significant growth from 2019 to 2032 where POC (point-of-care) testing consistently will hold a substantial share.[19] This growth highlights the increasing demand for rapid and accessible diagnostic solutions, reflecting advancements in technology and a shift towards decentralized healthcare.[19]

2.2 Biosensors

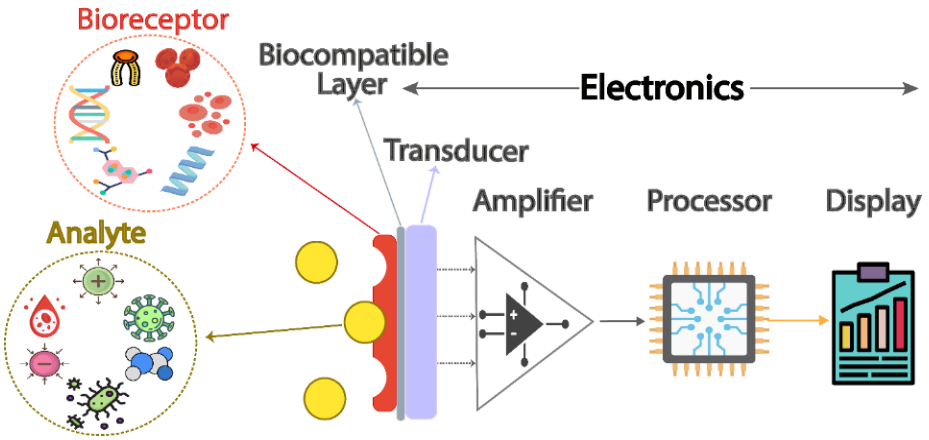

Figure 2: The components and process of a biosensor system are displayed, illustrating how a bioreceptor interacts with an analyte, with the response converted into a signal by a transducer. The signal is then amplified, processed, and displayed, highlighting the integration of biocompatible layers and electronics.

Biosensors are analytical devices that convert biological interaction into a readable signal, enabling the detection of specific analytes.[20-24] Its functional units comprise a bioreceptor, a transducer, and signal-processing components all integrated into a coordinated system as shown in Figure 2. The bioreceptor—such as enzymes, antibodies, nucleic acids, or molecularly imprinted polymers—interacts with the analyte via specific biochemical and biophysical mechanisms like enzyme-substrate binding, nucleic acid hybridization, or antigen-antibody recognition. [25-29] This interaction induces a physicochemical change which is detected and processed by the transducer (electrochemical, optical, piezoelectric, etc.), allowing for analyte quantification. The nature of the signal depends on the transduction mechanism used in the

biosensor. One can differentiate the signal based on their type and intensity to quantify the analyte. The signal from such elements is enhanced by an amplifier and processed by a processor to convert it into a readable format.[20] Finally, the results are shown on a display, often as graphs or numerical data.[20]

Electrochemical biosensors detect analytes by measuring changes in electrical properties upon interaction with the target molecule (or analyte) by deploying a biorecognition element. The measured changes in current (amperometry), voltage (potentiometry), or impedance (electrochemical impedance spectroscopy), where curves plotting peak current or impedance shift against analyte concentration enable quantification. This method is widely used for its sensitivity, specificity, and ability to provide real-time analysis.[12, 20, 22] For example, amperometric glucose sensors measure current generated by the enzymatic oxidation of glucose, where the resulting current peak height correlates with glucose concentration.[23] Potentiometric sensors, such as pH meters, track voltage changes proportional to ion concentration.[24]

Optical biosensors, such as fluorescence-based systems, detect changes in fluorescence intensity or wavelength. A DNA hybridization assay using fluorescently labeled aptamers shows increased fluorescence upon target binding, producing sigmoidal intensity-wavelength curves that quantify analyte concentration.[25, 26]

Nanopore-based systems record transient ion current blockades in resistive pulse sensing, where analytes like DNA strands transiently block ion currents as they pass through nanopores. The resulting current-time traces show characteristic blockage patterns (e.g., duration and amplitude), enabling single-molecule detection and sequencing.[27] Further sections focus on deeper explanation of the nanopore-based biosensors.

Lateral flow assays (LFAs) represent a widely used biosensor format that employs capillary action to transport samples across antibody-functionalized membranes. Unlike nanopore systems requiring sophisticated electronics, LFAs generate colorimetric signals through gold nanoparticle aggregation, visible as colored bands. While LFAs offer rapid results (<15 minutes) and simple visual interpretation (e.g., COVID-19 rapid tests), they lack the quantitative precision and single-molecule resolution of nanopore platforms.[24, 27]

The generated signals are processed by amplifiers and microprocessors, often visualized as calibration curves (e.g., current vs. concentration) or real-time kinetic plots (e.g., resonance angle vs. time), and displayed as numerical data or graphs for applications in medical diagnostics (e.g., glucose monitoring) and environmental toxin detection.[28, 29]

2.3 Nanopore Biosensors

Nanopore biosensors leverage unique physicochemical interactions between analytes and nanoscale pores to achieve molecular-level detection, distinguishing them from conventional biosensor architectures discussed in section 2.2. Their operation fundamentally depends on three interdependent parameters: nanopore dimensions, analyte geometry, and surface charge distribution. Size exclusion governs selective passage - molecules larger than the pore diameter are physically blocked, while smaller analytes translocate with characteristic ion current signatures shaped by their hydrodynamic radius and charge polarity. Conformational changes induced by analyte binding further modulate ionic conductance through charge redistribution or steric effects. Conversely, functionalized nanopores integrate biorecognition elements to combine physical sieving with biochemical specificity. In such cases a nanopore’s surface charge density and effective pore geometry amplify detection sensitivity.[30,

[31] This dual mechanism enables discrimination between similarly sized biomarkers such as IL-6 (21 kDa) and TNF-α (17 kDa) or Serum proteins (e.g., albumin, globulins) - a MoS_2/Al_2O_3 nanopore FET biosensor achieved 1 fg/mL prostate antigen detection by synergizing size exclusion with pore dimension constraints with antibody-antigen charge interactions.[32, 33]

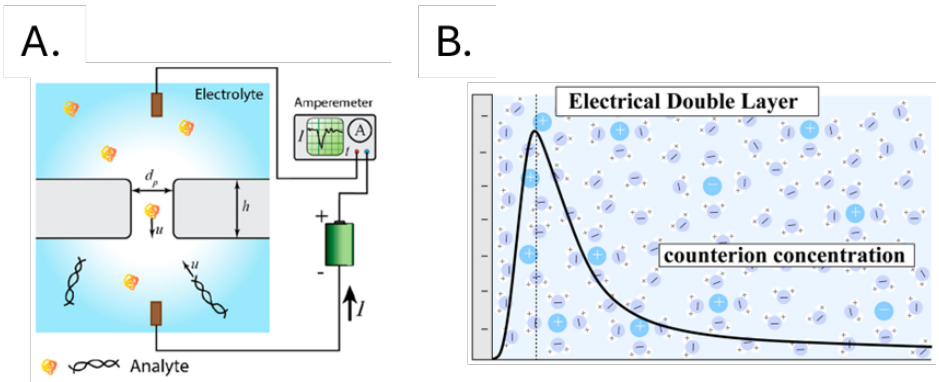

Figure 3: Schematic (A) illustration of a nanopore biosensor setup. Analytes (such as DNA and proteins) translocate through a nanopore embedded in a membrane separating two electrolyte chambers. An applied voltage drives ionic current through the pore, and analyte passage modulates the current, which is measured by an ammeter. Changes in the current provide information on the size, charge, and identity of the analyte. Adapted from ACS Sensors, 2021, 6, Wen, C.; Dematties, D.; Zhang, S. L., A Guide to Signal Processing Algorithms for Nanopore Sensors, 3536, with permission from ACS (CC-BY 4.0 license). (B) representation of the electrical double layer (EDL) at a charged surface in contact with an electrolyte solution. The graph shows the counterion concentration profile, highlighting the accumulation of counterions near the surface (forming the Stern layer) and the gradual decay into the bulk solution (diffuse layer). Adapted from Langmuir, 2015, Borwn, M; Bossa, G.; Guilherme, V; May, S., Emergence of a Stern Layer from the Incorporation of Hydration Interactions into the Gouy–Chapman Model of the Electrical Double Layer, 11477, with permission from ACS (CC-BY 4.0 license).

The electrical double layer (EDL,Figure 3) also plays a pivotal role in governing ionic conductance through nanopores. When a charged surface contacts an electrolyte solution, counterions accumulate near the surface to form the EDL, consisting of two regions: the tightly bound Stern layer and the more diffuse outer layer.[34, 35] In nanopores with dimensions comparable to the Debye length (characteristic thickness of the EDL), the EDL can occupy a significant portion or even the entire pore volume.[34] Such properties make nanopore biosensors transcend traditional biosensors by simultaneously exploiting nanoconfinement effects and molecular

recognition, enabling ultrasensitive quantification in complex matrices like serum or saliva.

The outlined reasons showcase nanopore biosensors as powerful emerging tools for point-of-care (POC) diagnostics because of their ability to detect single molecules with high sensitivity and specificity.[36, 37] They have demonstrated remarkable diagnostic capabilities comparable to gold-standard methods. An analysis of 297 infectious fluid samples found nanopore sequencing technology (NST) achieved 100% positive predictive agreement with conventional culture methods in microbial-colonized sites like respiratory and urinary tracts, alongside 95% negative predictive agreement in cerebrospinal fluid samples.[38] This high accuracy, combined with advantages such as real-time pathogen identification, detection of antimicrobial resistance genes, and portability, positions nanopore biosensors as promising alternatives to traditional diagnostic methods in point-of-care settings. Similarly, a study applied high-throughput nanopore sequencing to characterize phage display antigen-binding fragments (Fabs) libraries, using an in-lab sequencing device (by Oxford Nanopore) to comprehensively analyze library composition throughout selection processes.[39] This approach allowed for rapid, large-scale analysis of antibody sequences. Field-effect transistor (FET) biosensors operate by detecting minute electrical changes when target biomarkers bind to their surface. Another study utilized a nanoporous molybdenum disulfide (MoS_2) channel – engineered with aluminum oxide (Al_2O_3) encapsulation – to serve as the sensing element for prostate cancer biomarkers. The FET's conductivity shifts as prostate-specific antigens attach to the MoS_2 pores, enabling ultrasensitive detection down to 1 fg mL^{-1}.[40] Such nanopore-based biosensing systems demonstrate selective detection of active biomarkers in a high-throughput manner from diverse samples including saliva, cerebrospinal fluid, blood plasma, and bacteriophages. These advancements alongside several other

studies underscore the potential of nanopore biosensors in revolutionizing rapid, accurate, and accessible diagnostic tools across various medical fields.[41-44]

2.4 Copper-binding Moieties

Copper is an essential trace element that plays a crucial role in various biological processes, including energy production, antioxidant defense, and neurotransmitter synthesis.[1] However, maintaining proper copper homeostasis is critical because deficiency and excess can lead to severe health consequences. Copper deficiency can impair immune function, neurological development, and hematopoiesis, whereas copper overload can cause oxidative stress, tissue damage, and organ dysfunction, particularly in the liver and brain.[2] The dysregulation of copper homeostasis has been implicated in several disorders, including Menkes disease, Wilson's disease, and neurodegenerative conditions, such as Alzheimer's disease.[45] Given the critical importance of maintaining appropriate copper levels in the body, accurate and sensitive detection of copper ions, particularly in human serum, is essential for early diagnosis, treatment monitoring, and understanding the pathophysiology of copper-related disorders.

In this regard broader biological copper-binding systems, such as natural proteins that leverage cooperative or competitive binding mechanisms, are key to building biosensors for its detection. Further, Table 1 shows synthetically engineered peptides and MOFs exploit structural motifs or hybrid inorganic-organic architectures for targeted copper interactions in physiological or environmental applications. Recent research has also focused on developing more selective and sensitive copper-binding peptides.

Table 1. Summary of Copper-Binding Moieties

Type	Example	Binding Sequence/ Structure	Binding Properties
Proteins	Ceruloplasmin	Six Cu-binding sites	Cooperative binding; non-exchangeable Cu ions.[46]
	Prion Protein	HGGGW (octarepeat sequence)	Coordination via histidine imidazole and glycine carbonyls.[47]
	Human Serum Albumin	Specific binding sites	Competes with free amino acids like histidine for Cu(II).
Peptides	GHK-Cu	Gly-His-Lys	High affinity for Cu(II); regulates gene expression.[48]
	ATCUN Motif	N-terminal sequence	Selective binding; used in sensing applications.[49]
MOFs	Cu-MOF-808	Zr_6O_8 clusters	Strong metal-bonding interactions; luminescence quenching upon NO2 adsorption.[50]
	Cu@Ni-MOF-74	Ni-MOF framework	Enhanced CO/N2 separation; optimized Cu impregnation.[51]

The Amino-Terminal Cu(II)- and Ni(II)-binding motif (ATCUN) has been extensively studied and optimized for copper sensing applications.[52] Modifications to these peptides, such as the incorporation of non-natural amino acids or the optimization of fluorescent labels, have led to improved binding affinities and signal transduction.[52]

2.5 Peptides on Nanopores

Recent research has focused on advanced nanopore-based biosensing by integrating peptide probes and nanobodies for ultrasensitive protein detection. One approach employs nanobody-functionalized synthetic nanopores, where directional immobilization of nanobodies via copper-free click chemistry enables selective recognition of proteins like green fluorescent protein (GFP), mCherry, and α-amylase.[53] This system combines optical and electrical readouts to generate dose-response curves, leveraging changes in surface charge density within nanoconfined geometries to detect analytes at physiologically relevant concentrations.[53] A complementary strategy utilizes dual-nanopore biosensors with affinity-tunable peptide probes for label-free monitoring (i.e., detection without fluorescent tags or chemical labeling) of the protein kinase A (PKA) catalytic subunit in single live cells. By screening peptide probes with optimized binding affinities, this platform achieves a detection limit of 0.04 nM for PKA, resolving dynamic concentration changes during cellular stimulation while the spatiotemporal resolution allows tracking of proteins abundance fluctuations in real time, demonstrating precise monitoring of PKA activity under pharmacological interventions in intact cellular environments.[54] Another innovative design incorporates peptide nucleic acid (PNA) segments covalently linked via amide bonds to ion channel-forming alamethicin monomers—a 20-residue peptaibol with an α-aminoisobutyric acid (Aib)-rich sequence.[55-57] These chimeric molecules exploit PNA's sequence-specific hybridization with single-stranded DNA fragments (e.g., cell-free DNA from serum samples) to modulate alamethicin nanopore conductivity, enabling selective detection through characteristic current disruptions during DNA-PNA binding events.[55, 58] The integration of peptides with nanopores offers distinct advantages compared to traditional biosensing platforms (e.g., antibody-based assays or unmodified nanopores), particularly through enhanced

molecular recognition capabilities and tailored functionality. While conventional biosensors often require extensive sample preprocessing or lack modularity, peptide-modified nanopores enable target-specific interactions through programmable peptide sequences that recognize biomarkers, pathogens, or environmental contaminants with high affinity.[59] This contrasts with non-functionalized nanopores, which primarily rely on physical parameters like size exclusion or charge-based discrimination, limiting their applicability to structurally well-defined analytes.[59] The technology shows great potential for applications in various fields, such as disease diagnosis, environmental monitoring, and DNA sequencing.[60, 61]

Studies describe advancements in nanopore-only detection systems, which utilize materials such as poly(ethylene terephthalate) (PET), polycarbonate, and SiO_2 for track-etched membranes.[62, 63] Ion-track etching enables precise control over pore geometry (e.g., conical or cylindrical shapes) and size distributions (2–18% variability depending on material). These membranes serve as robust substrates due to their chemical stability, tunable surface charge, and compatibility with functionalization strategies.[62, 64] For instance, PET track-etched membranes modified with polyacrylic acid or 4-vinylpyridine have demonstrated ultrasensitive detection of heavy metal ions (e.g., Cu^{2+}, Pb^{2+}) at µg/L concentrations.[65] Similarly, graphene oxide-polycarbonate hybrid nanosieves achieved femtomolar sensitivity for HIV glycoprotein detection through covalent receptor immobilization of the ion-track etched membranes.[66]

2.6 Transduction by Voltammetry - Fluorescence

Voltammetry is an electrochemical technique used in biosensing to measure the current response of an analyte over a range of applied voltages, as shown in Figure 4.A.[67] It is particularly useful for detecting redox-active species and provides valuable information

about the analyte's concentration and kinetics.[67-69] This technique was employed to characterize and optimize the functional layers of the xanthine biosensor design, which included a xerogel with and without embedded xanthine oxidase enzyme (XOx) and an outer, semi-permeable blended polyurethane layer.[67] The study demonstrated that doping the xerogel layer with different alkanethiol protected gold nanoparticles (Au-NPs) enhanced biosensor performance, including improved sensitivity, linear range, and response time, while also stabilizing xanthine sensitivity and discrimination against common interferent species over time.[67]

Fluorescent labeling of peptides has emerged as a cornerstone in biosensing, enabling real-time monitoring of molecular interactions through optical readouts. State-of-the-art approaches often employ environment-sensitive fluorophores or Förster resonance energy transfer (FRET) pairs, where analyte binding induces conformational changes or proximity-dependent quenching (on-off state shown in Figure 4.B).[70, 71] For metal ion detection, coordination-sensitive probes like coumarin derivatives or dansyl tags are widely used, as their fluorescence is modulated by metal-induced electron transfer or chelation-enhanced quenching.[72, 73] Another study exemplifies the synergy between nanopore functionalization and optical sensing wherein conjugating nanobodies to track-etched nanopores via click chemistry, dual optical-electrical detection of proteins like α-amylase was achieved.[53]

Among the examples which combine nanopore based electrochemical/fluorescence detection are represented by recent

developments in the Tietze Lab and will be described in detail in chapter 4.

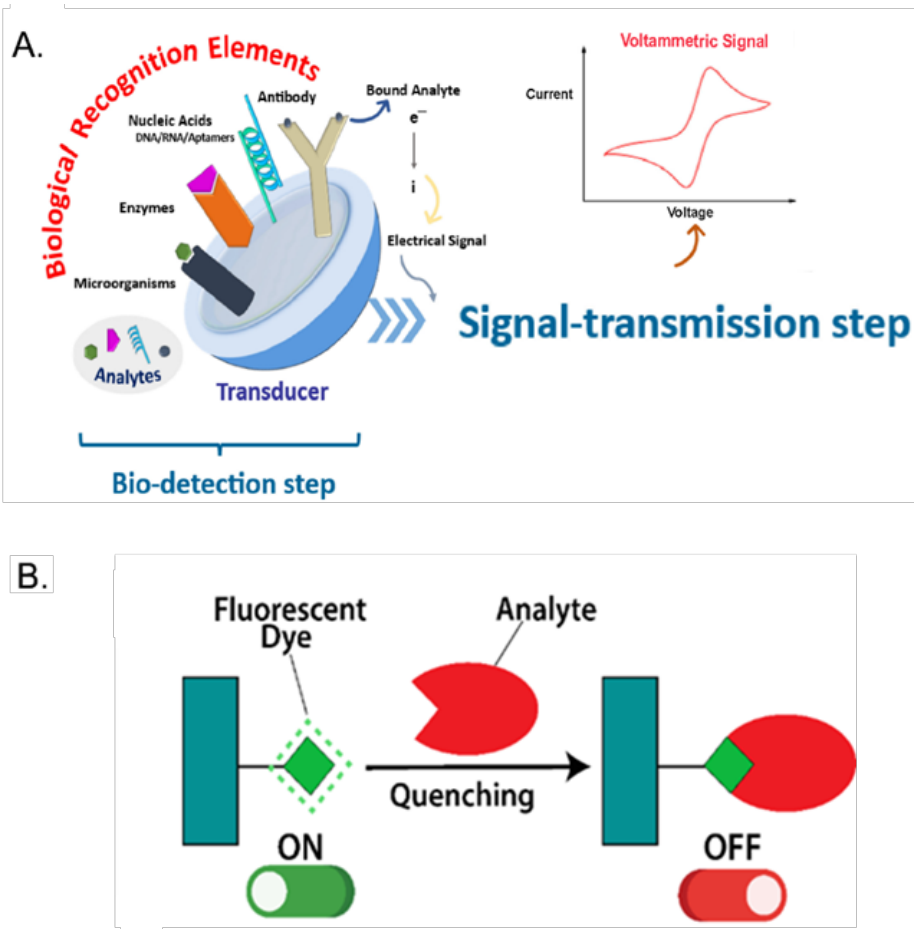

Figure 4: (A) Illustration detailing the complete process of electrochemical biosensing, emphasizing the role of biological recognition elements and signal processing along with the characteristic voltammetric signal illustrating how current varies with applied voltage. This response provides insights into the concentration and kinetics of the analyte, demonstrating the sensor's sensitivity and specificity. Adapted from Chemical Engineering Journal Advances, 2023, 16, Shanbhag, M. M.; Manasa, G.; Mascarenhas, R. J.; Mondal, K.; Shetti, N. P., Fundamentals of bio-electrochemical sensing, 100516, with permission from Elsevier (CC BY-NC-ND 4.0 license). (B) Illustration of fluorescence quenching mechanism used in sensing applications. Initially, the fluorescent dye is in an "ON" state, emitting light. The analyte interacts with the fluorescent dye by attaching to it. This interaction leads to quenching, where the fluorescence is reduced or turned "OFF." The presence of the analyte is detected by the change from the "ON" to "OFF" state, indicated the analogous on-off switch mechanism associated with the quenching.

2.7 ATCUN functionalized Nanopore

The ATCUN (Amino Terminal Cu(II) and Ni(II) binding) motif is derived from the protein sequence and is known to exhibit high specificity for binding metal ions, such as copper and nickel, making it an excellent candidate for various applications in spectroscopy, imaging, and biosensor design.[74] The ATCUN motif typically consists of a three-amino acid sequence at the N-terminus of a peptide, with the general structure Xaa-Xaa-His, where Xaa can be any amino acid and His is histidine. This specific arrangement allows for the formation of a square planar complex with metal ions upon binding, primarily Cu(II) and Ni(II), through coordination with the N-terminal amine, two deprotonated amide nitrogen, and the imidazole side chain of histidine(Figure 5.A).[75] Structural studies on ATCUN demonstrate that sequence variations like the addition of a second histidine residue at position 1 or 2 (e.g., HWHG and HGHW) enhance Cu(II) uptake kinetics without altering thermodynamic stability. Further, modifications such as phosphorylation of residues adjacent to the ATCUN motif have been shown to weaken Cu(II) binding affinity by disrupting coordination geometry.[76, 77] This conformational change often leads to alterations in the electronic and structural properties of the peptide, which can be exploited for sensing purposes as also utilized in this thesis.[41, 42, 75] The understanding of optimal binding conditions for selective binding of ATCUN motif to the Cu(II) ion is crucial for the biosensor development process.

Functionalization of ATCUN peptides to ion-track etched membranes with nanopores creates a robust biosensor platform capable of detecting metal-ions at low concentrations as illustrated in Figure 5.A.[60, 78] These peptides, when anchored to nanopore surfaces, enable metal-ion-selective binding and redox-active sensing, leveraging their innate coordination chemistry to enhance specificity for targets like transition metals or metalloproteins.[64, 79] This approach capitalizes on the synergy between the nanopore's

single-molecule resolution and the peptide's molecular recognition properties, as exemplified in the Tietze Lab's work on Cu^{2+} detection using ATCUN functionalized membranes. Such systems bypass the limitations of non-functionalized nanopores, which lack intrinsic biorecognition elements, and traditional biosensors, which suffer from slow throughput and complex workflows.

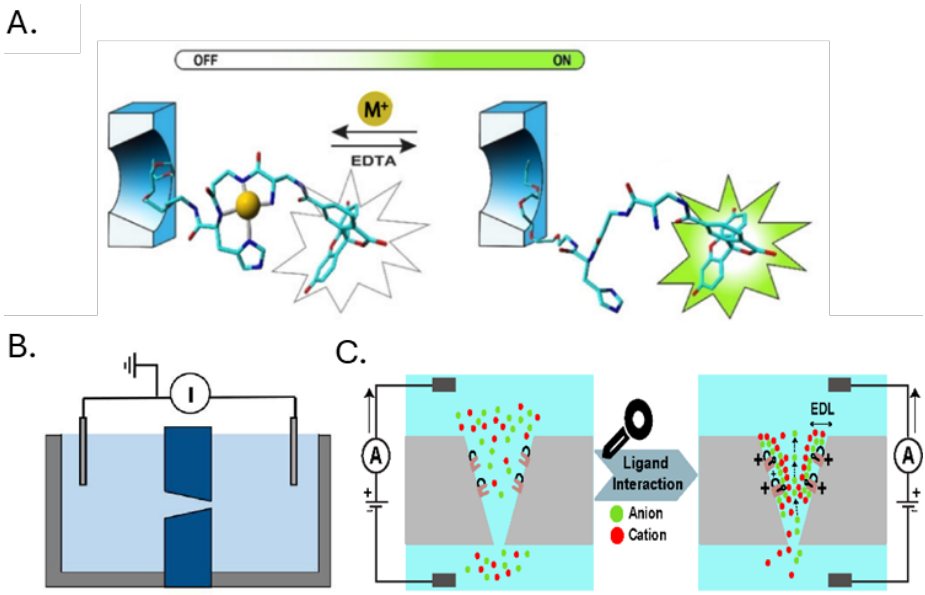

Figure 5: (A) Schematics of a fluorescently labelled ATCUN peptide functionalized on a nanopore. The ATCUN motif binds metal ions, such as copper (M^+), resulting in a conformational change that enhances fluorescence quenching. This process is crucial for developing biosensors with high sensitivity and selectivity for metal ion detection. Adapted from Chemistry-A European Journal, 26 (39), Muller, L. K.; Duznovic, I.; Tietze, D.; Weber, W.; Ali, M.; Stein, V.; Ensinger, W.; Tietze, A. A., Ultrasensitive and Selective copper(II) Detection: Introducing a Bioinspired and Robust Sensor 2020, 8511-8517, with permission from Wiley. (B) Schematics of the Electrochemical Cell Setup with Nanopore Membrane, with permission from Darmstadt University and State Library Darmstadt (CC BY-NC-ND 4.0 license). (C) Lock-and-key mechanism in ATCUN-nanopore ion transport. Before ligand interaction, the nanopore shows balanced ion distribution with limited conductance. After Cu(II) (key) binds to ATCUN peptides (lock), positive charges form an electrical double layer (EDL) which creates an anion-selective channel, dramatically increasing current flow. This lock-and-key interaction transforms the nanopore from a non-conductive state to a highly conductive one, enabling sensitive Cu(II) detection through measurable changes in IV curves.

Figure 5.B illustrates the basic electrochemical cell schematic used in this thesis, which involves two electrodes immersed in an electrolyte solution. A potential is applied across the electrodes, and the resulting current is measured.[64, 80] The nanopore membrane at

the center of the electrodes plays a crucial role by allowing selective passage of ions, which is essential for detecting specific analytes through changes in their electrical properties. Before Cu(II) binding occurs, the modified nanopore exists in a "rectifying" state that restricts anion passage, effectively functioning in an "off" state with minimal current flow (Figure 5.C Left).[64] When Cu(II) ions bind to the ATCUN crafted onto the nanopore walls, they generate positively charged complexes that fundamentally modifies the surface charge density of the nanopore (Figure 5.C Right).[64] The redistribution of ions within the EDL (Electric Double Layer) leads to increased ionic conductance (Figure 5.C Right). The positively charged complexes attract anions (e.g., Cl^- or SO_4^{2-}), which accumulate near the pore walls and enhance anion transport through the pore. This effect is amplified as more Cu(II) ions bind to ATCUN peptides, progressively increasing the positive charge density and strengthening anion selectivity. With increasing Cu(II) concentrations, the local ionic strength near the nanopore surface rises due to the accumulation of counter-ions in response to newly formed positive charges. Higher ionic strength reduces the Debye length by compressing the diffuse layer and concentrating ion transport closer to the pore walls. The Debye length is inversely proportional to the square root of ionic strength. This compression further enhances current flow by reducing resistance within the nanopore. This shift to anion selectivity manifests as a progressive increase in current that correlates directly with increasing Cu(II) concentration.[64]

Fluorescence-based biosensors utilize the emission of light by fluorophores upon excitation to detect target molecules.[81, 82] This method is highly sensitive and can be used to monitor biological interactions in real-time.[83, 84] Fluorescence quenching occurs when the fluorescence of a dye (Figure 4.B) is reduced due to interaction with a quencher, such as a metal-ion.[85, 86] This principle is used in biosensing to detect the presence of specific analytes by observing

changes in fluorescence intensity , as presented in this thesis.[87, 88] In the context of this thesis, ATCUN peptides functionalized with fluorophores like 6-carboxyfluorescein or Rhodamine B provide a quenching-based Cu(II) sensing platform. The quenching mechanism in ATCUN peptide-Cu(II) systems arises from photoinduced electron transfer (PET), where Cu(II) acts as an electron acceptor. Upon binding to the ATCUN motif's N-terminal tripeptide sequence, Cu(II) facilitates non-radiative decay of the fluorophore's excited-state electrons, effectively suppressing fluorescence emission.[73, 89] The PET mechanism between the fluorophore and Cu(II)-ATCUN complex allows quantification of Cu(II) concentrations via dose-dependent fluorescence attenuation.[41-44]

2.8 Signal Quantification: from raw data to insights

Beyond the design and selection of the biosensors, their performance relies on robust methods to translate raw signals (e.g., current, fluorescence) into analyte concentrations. This is typically achieved through the construction of calibration curves, where signals from known analyte concentrations are recorded and used to establish a mathematical relationship between signal output and concentration. Linear calibration models are employed when the response is directly proportional across the concentration range; however, many biosensing applications, particularly those involving

cooperative binding or multi-step interactions, are better represented by sigmoidal models.

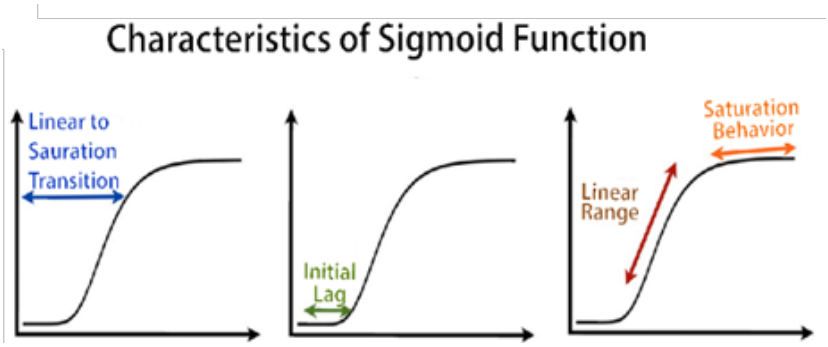

Figure 6: Illustration of Sigmoid function with three similar characteristics: 1) an Initial Lag or period of Slow Growth, 2) Rapid Linear Range, and 3) a period of Reduced Growth-Rate (Saturation Behaviour). Adapted from NeuroImage, 2014, 84(742), Douglas, D. C.; O' Muircheartaigh, J.; Dirks, H.; Waskiewicz, N.; Lehman, K.; Walker, L.; Han, M. ; Deani, S., Modeling healthy male white matter and myelin development: 3 through 60 months of age, with permission from Elsevier (CC BY-NC-ND 4.0 license).

These S-shaped curves (Figure 6) are prevalent in biosensing because they effectively model various binding phenomena, including cooperative interactions, allosteric regulation, and multi-step binding processes such as those observed in ATCUN-metal systems and other ligand-receptor interactions.[90-92] These mathematical representations capture both the threshold response and saturation behavior common in molecular recognition events, providing crucial insights into underlying biological or chemical mechanisms essential for understanding sensor performance and optimizing design.[93,91] Such dose-response modeling proves particularly valuable in biochemical diagnostic procedures where the relationship between analyte concentration and signal output forms the basis of detection.[92,94] In cases of asymmetry, a four-parameter logistic (4PL) or five-parameter logistic (5PL) curve have shown to be accurate ways to represent these relationships.[94] Using sigmoidal models like the 4PL or 5PL for calibration curves in biosensors can lead to more accurate determination of important parameters such as the limit of detection (LOD).[92, 94] For example, in a study on the detection of squamous cell carcinoma antigen

using a surface plasmon resonance biosensor, the 4PL model yielded more precise LOD values compared to classical methods.[92]

Recent reports highlight various approaches to validate biosensor efficacy across different applications. In a study on transdermal alcohol biosensors, researchers employed time-series models to compare the temporal dynamics of wrist-worn sensors with traditional ankle monitors. The analysis revealed that the new-generation wrist-worn sensor detected alcohol peaks over an hour earlier than its counterpart.[95] Another study utilized multiple statistical models (partial least squares, random forest, elastic net, and C5.0) to build diagnostic classifiers for autism spectrum disorder based on biosensor data. Model performance was evaluated using receiver operating characteristics (ROC) and kappa statistics, demonstrating moderate discriminatory power between autism spectrum disorder and typically developing participants.[96] In the context of COVID-19 forecasting, researchers compared the m-ADBio model with the traditional SEIR model using statistical significance testing. The results showed no statistically significant difference between the m-ADBio model's forecasts and observed data at the community level, indicating high accuracy.[97]

When signal differences are minimal or data complexity increases—such as at very low analyte concentrations or in complex biological matrices—machine learning algorithms become valuable tools for improving interpretation. These algorithms can process multimodal and nonlinear data, identifying subtle patterns that traditional calibration approaches might miss, thus maintaining sensitivity and accuracy across a broader concentration range.[98] The integration of machine learning with conventional calibration models has been shown to enhance prediction accuracy, particularly in challenging analytical scenarios.[99] This process is essential for optimizing sensor design and functionality, making the application of machine learning techniques more effective.[98]

2.8.1 Machine Learning

Machine learning is a branch of artificial intelligence that enables systems to learn and improve from experience without being explicitly programed.[100, 101] Unsupervised learning involves training algorithms on data without labeled responses, which allows the model to identify patterns and structures. Principal Component Analysis (PCA) is an unsupervised learning technique used to reduce data dimensionality while preserving variance (Figure 7.E). This technique is relied upon in this study because it is commonly used in biosciences to identify patterns and trends in complex datasets.[100, 102] Supervised learning is a type of machine learning in which models are trained on labeled data to make predictions or decisions. Labeled data refers to datasets that include input features paired with corresponding output values (labels) that indicate the correct prediction or classification for each example. It includes various algorithms, such as decision tree, logistic regression, neural network, naive bayes, boosting.

Decision tree is a binary tree structure used for classification and regression. It splits data into branches based on feature thresholds, which allows intuitive decision-making processes(Figure 7.A).[103, 104] Logistic regression is used for binary classification tasks. It models the probability that a given input belongs to a particular category and is particularly useful when the relationship between features and target variable is linear. Logistic regression is a popular choice in applications because it can handle binary outcomes and provide probabilistic predictions(Figure 7.B).[103, 105] Neural network is a machine learning model inspired by the human brain comprising of interconnected nodes (neurons) organized in layers. It can learn complex patterns from data through a process called

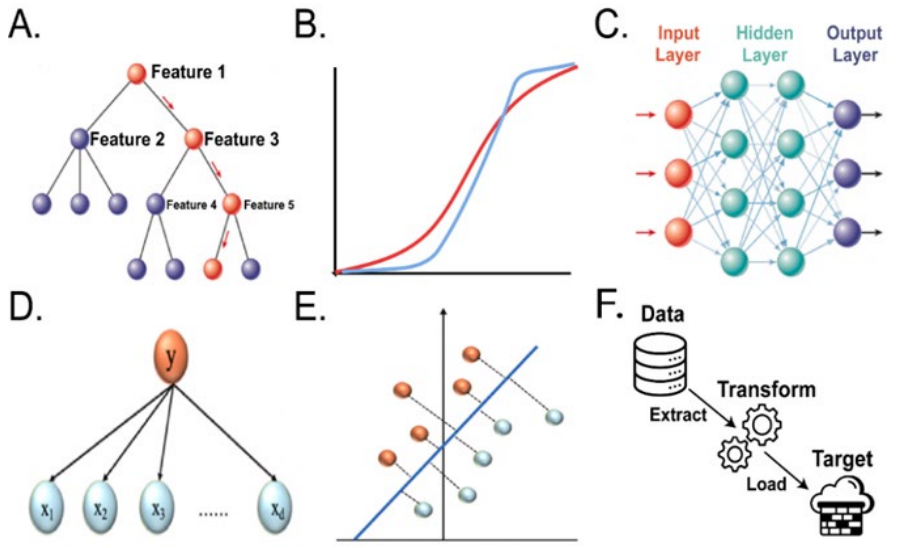

Figure 7: Illustration of machine learning algorithms such as (A) Decision Tree: where features are used to make decisions at each node. The tree branches out based on feature values, ultimately leading to a decision or classification. (B) Logistic Regression: a statistical method used for classification. The S-shaped curve shows how the probability of an outcome changes with the input features. (C) Neural Network: The diagram shows a multilayer perceptron architecture with input, hidden, and output layers. Each layer is composed of nodes that are interconnected, demonstrating that the data flows forward unidirectionally, through the network for processing and learning. (D) Naive Bayes Algorithm: which is based on applying Bayes' theorem with strong independence assumptions between features. It is commonly used for classification and other probabilistic tasks. (E) Principal Component Analysis (PCA): a dimensionality reduction technique that transforms data into a new coordinate system. The principal components are shown as axes, capturing the directions of maximum variance in the data. (F) ETL Process (Extract, Transform, Load): This flowchart outlines the ETL process used in data warehousing and integration. Data is extracted from various sources, transformed into a suitable format, and loaded into a target system for analysis. Adapted from Current Research in Food Science, Volume 8, Zhou, Z.; Tian, D.; Yang, Y.; Cui, H.; Li, Y.; Ren, S.; Han, T.; Gao, Z., Machine learning assisted biosensing technology: An emerging powerful tool for improving the intelligence of food safety detection, with permission from Elsevier.

backpropagation, by adjusting its internal parameters to minimize prediction errors. They are versatile and can be applied to various biosensing tasks, including classification, regression, and pattern recognition (Figure 7.C).[103, 106, 107] Naive Bayes is a probabilistic classifier based on Bayes' theorem, assuming independence between features (Figure 7.D). It is highly efficient for large datasets and performs well with categorical data.[103, 108] Neural Boosting is an ensemble learning technique that combines multiple weak learners to form a strong learner. It iteratively adjusts the weights of weak learners based on their performance, improving overall accuracy.[103, 109]

Deep learning utilizes neural networks with multiple layers to learn effectively from data. Within biosensors, neural network algorithms have been instrumental in improving sensitivity, selectivity, and accuracy.[110-112] The Multilayer Perceptron (MLP) is a type of Feed Forward Neural Network (FNNN) within deep learning model that consists of an input layer, one or more hidden layers, and an output layer(Figure 7.C).[112, 113] It is capable of capturing complex non-linear relationships between inputs and outputs, making it a powerful tool for biosensor data analysis.[100, 114, 115]

Extract Transform Load (ETL) Pipeline process involves extracting data from various sources, transforming it into a suitable format, and loading it into a data warehouse for analysis(Figure 7.F).[116, 117] This process is already an essential practice for managing and analyzing large volumes of medical or clinical data efficiently.[118-120] The ETL process plays a vital role in data warehouse architecture, enabling effective decision-support implementation and maintaining data integrity.[117, 121]

2.9 From manual to automated screening

Manual measurements in biosensor development involve the direct handling of samples and reagents, typically requiring human intervention for tasks such as pipetting, mixing, and data recording. For instance, fluorescence-based biosensors and surface plasmon resonance (SPR) sensors are commonly used in environmental monitoring to detect water pollutants manually. These methods often rely on visual or spectroscopic readouts, with researchers manually preparing samples and interpreting results. SPR biosensors, for example, have been widely employed due to their high sensitivity, but they require precise manual calibration and handling to achieve optimal detection limits. At the Tietze lab, the development of the ATCUN nanopore-based based biosensor for detecting copper(II) ions initially utilized traditional setups such as measurement cells with electrolyte solution and confocal laser

scanning microscopy (CLSM) for I-V and fluorescence measurements, respectively.[44, 64] This allowed for high-resolution imaging of molecular interactions alongside precise electrochemical measurements. Such dual detection workflows are particularly useful for studying complex biosensor designs where both optical and electrochemical properties are critical. However, due to the manual nature of these workflows, such sophisticated operations can be labor-intensive and prone to variability due to manual errors.

Automation significantly enhances the efficiency and reliability of these processes. Automated testing platforms streamline repetitive tasks such as liquid handling, sample preparation, and data acquisition, enabling simultaneous testing of multiple samples. These platforms allow for the simultaneous testing of multiple samples, speeding up the development cycle.[122, 123] They enhance precision as automation reduces human error, ensuring consistent and accurate results across experiments. Automated systems optimize resource usage by minimizing the manual handling of samples and reagents, thereby reducing waste and lower costs.[124] They facilitate innovation with faster testing and iteration, researchers can explore a wider range of designs and materials, leading to more innovative biosensor solutions.[125, 126]

The incorporation of sophisticated technologies such as robotics, precision dispensing mechanisms, and integrated software for task automation with liquid handling systems makes them truly advanced in capability (Figure 8.A). Such systems automate the precise delivery and mixing of reagents, which are crucial for high-throughput biosensor screening.[127] These systems ensure repeatability and accuracy in experimental conditions, facilitating the development of reliable biosensors.[125-127]

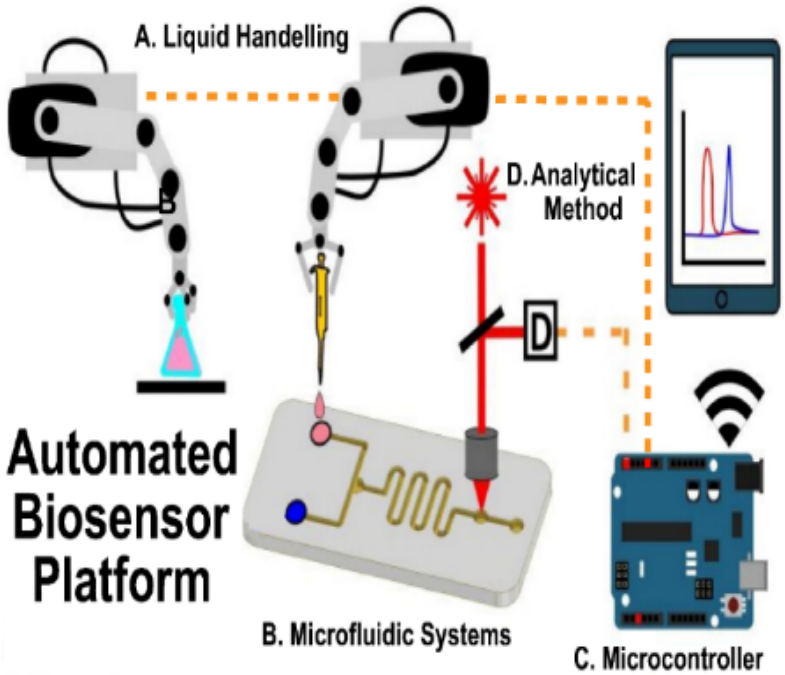

Figure 8: Schematic illustration of a typical automated biosensor platform featuring robotic arms for (A) liquid handling, (B) a microfluidic system for precise sample processing. The setup also includes a (C) microcontroller and (D) an analytical method for data generation and analysis, with results displayed on a digital device. Adapted from ACS Sensors, 9 (3), Raju, C. M.; Elpa, D. P.; Urban, P. L., Automation and Computerization of (Bio)sensing Systems. 2024, 1033-1048, with permission from ACS.

2.9.1 Microfluidics in Automated Platforms

In particular, the incorporation of microfluidics into automated testing platforms allow for real-time analysis and seamless integration with electronic components, making them particularly suitable for point-of-care diagnostics due to reduced sample consumption and increased sensitivity (Figure 8.B). They enable

precise control over fluid handling and enhance the integration of biosensors with electronic systems, making them ideal for point-of-care diagnostics.[128, 129]

For example, robotic digital microfluidics (RDMF) platforms have been developed to manipulate droplets mechanically on superhydrophobic cartridges. These systems perform diverse operations such as droplet dispensing, mixing, and splitting, all while integrating detection techniques like urinalysis tests with high precision and versatility.[130] Similarly, optofluidic biosensing platforms combine advanced microfluidic techniques with photonic components to study diseases at the molecular level.[131, 132] Such setups integrate micro-pumps and valves with optical resonators, enabling label-free detection methods that are compact and efficient.[133] Microfluidics enhances automation by enabling miniaturization and integration with complementary microsystems. For instance, automated microfluidic chips used in next-generation sequencing (NGS) streamline DNA library preparation by combining magnetic bead transport with electrokinetic flow. This reduces reagent use and manual intervention while maintaining high sequencing accuracy.[134, 135] Furthermore, paper-based microfluidics has simplified isothermal nucleic acid amplification tests by automating nucleic acid extraction, amplification, and detection processes on a single platform. These systems are particularly valuable for low-resource settings due to their cost-effectiveness and ease of use.[136, 137] By seamlessly merging microfluidics with automated setups, researchers can achieve higher throughput, greater reproducibility, and faster iteration cycles, paving the way for innovative biosensor solutions that address complex analytical challenges.

Chapter 3

3.0 Finding the Optimal Protocol for Coupling Various Dyes to ATCUN-like Structures (Paper I)

In chapter 2 the state-of-the art status of the development of fluorescently labeled ATCUN peptide has been described in section 2.7. Starting from there, we explored if other fluorescence dyes could increase the performance of the peptide, namely if quenching properties could be enhanced depending on the type of the dye attached to ATCUN. In this regard, three different dyes were tested in Paper I, namely 6-carboxyfluorescein (FAM),[138] Rhodamine B (RhoB),[139] and 4,4-Difluoro-4-bora-3a,4a-diaza-s-indacene propanoic acid (BODIPY-FL).[140]

Further, the optimal protocol for coupling the dyes to ATCUN was also studied since it was a yield limiting step. The ATCUN peptides, represented in Figure 9.A were synthesized using a standard Fmoc-based protocol solid-phase peptide synthesis (SPPS) on Gly-preloaded Wang resin.[41]

3.1 ATCUN-Fluorophore Coupling Optimization

The study compares conventional peptide coupling reagents (HATU, HBTU, PyBOP) with pentafluorophenol (PFP) esters activated by 1-ethyl-3-(3-dimethylaminopropyl)carbodiimide (EDC) for labeling primary amines on ATCUN peptides using fluorescein (FAM), Rhodamine B (RhoB), and BODIPY-FL dyes. Conventional

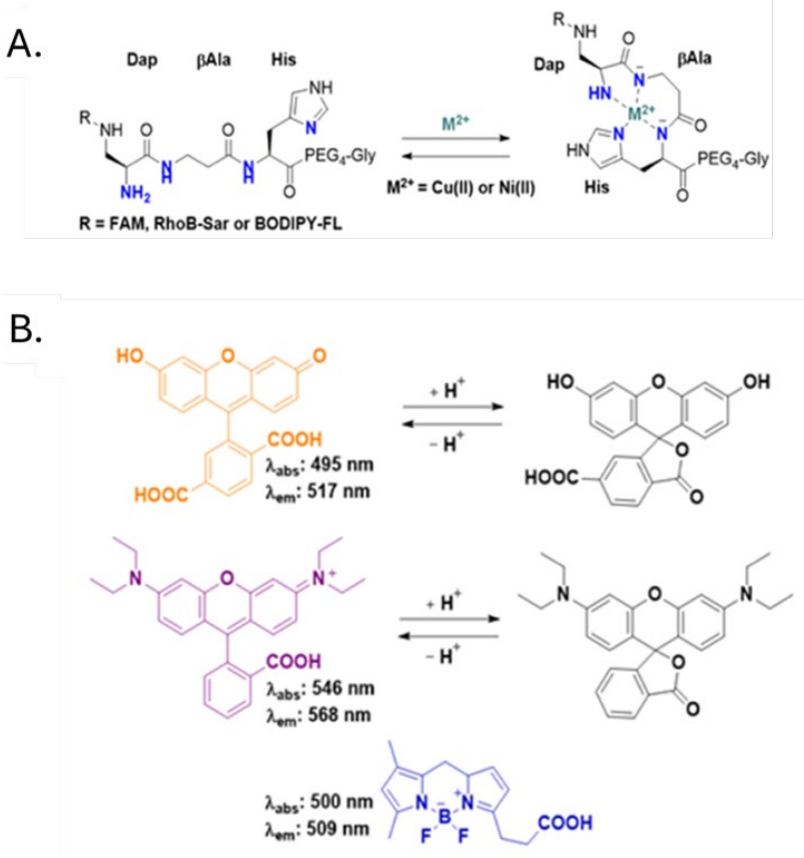

Figure 9: (A) Metal-ion Binding to Peptide Conjugates: Complexation behavior of the ATCUN motif Dap-β-Ala-His with Cu(II) or Ni(II), the coordinating nitrogen atoms are highlighted in blue. (B) Characterization of Metal-ion Interactions with Fluorophores and Peptide Conjugates. Structures of FAM (top, orange), RhoB (middle, purple), and BODIPY-FL (bottom, blue), including spirolactamization of RhoB and FAM, leading to their respective non-fluorescent isomers, Adapted from ACS Organic & Inorganic Au 2024, Volume 4, Issue 5, Hintzen, J. C. J.; Devrani, S.; Carrod, A. J.; Bayik, M. B.; Tietze, D.; Tietze, A. A., Fluorescence Labeling of Peptides: Finding the Optimal Protocol for Coupling Various Dyes to ATCUN-like Structures, with permission from ACS.

methods show low efficiency, with yields of 3–10% for FAM-ATCUN-Gly and trace–6% for BODIPY-ATCUN-Gly (see Table 2). In contrast, PFP/EDC significantly improves yields due to enhanced activation kinetics and reduced steric hindrance as shown in Table 2. For example, FAM-ATCUN-Gly synthesis achieved 44% yield with PFP/EDC versus 3% with HATU/HBTU. Similarly, BODIPY-FL labeling efficiency rose from ≤1% (HATU/PyBOP) to 44% when PFP/EDC was combined with microwave irradiation (80°C, 10 min), which accelerated ester formation.[41]

For secondary amines (e.g., sarcosine-modified peptides), conventional reagents like PyBOP performed better (29% yield for RhoB-Sar-ATCUN-Gly, see Table 2), highlighting context-dependent optimization. The PFP/EDC strategy's efficacy stems from its ability to form stable active esters, minimizing side reactions and enabling scalable synthesis under mild conditions. This approach expands the toolkit for developing fluorescent ATCUN-based biosensors, particularly for Cu(II)/Ni(II) detection, without compromising metal-binding or quenching properties.

In particular, while conjugating Rhodamine B to the primary amine of ATCUN peptides, we observe spirolactamization (Figure 9B).[41] This compromised fluorescence quenching by locking the dye into a non-fluorescent closed-ring conformation. This structural transformation prevented the fluorophore from existing in its open-chain fluorescent state, which is essential for metal-induced quenching through electron/energy transfer mechanisms. As a result, the quenching efficiency decreased significantly because the spirolactam form remains optically inactive even after Cu(II)/Ni(II) binding to the ATCUN motif. This issue was resolved by introducing sarcosine as a spacer, preventing the formation of the non-fluorescent spirolactam form.[41] The prevention of unwanted side reactions, such as spirolactamization in RhoB-labeled peptides, leads to more stable biosensors with consistent performance over time and potential for long-term storage and repeated use without significant degradation. Therefore, the linker length between the fluorophore and the ATCUN motif is an important parameter, which affects fluorescence quenching efficiency. Increasing the linker length prevents spirolactamization but reduces quenching efficiency by Cu(II) binding. However, it did not affect metal-binding constants.[41] This finding highlights the importance of optimizing the spatial relationship between the fluorophore and the metal-binding site for maximum sensor performance.

Table 2. Comparison of Dye Labeling Yields for ATCUN Peptides

Coupling Method	FAM-ATCUN-Gly Yield	RhoB-ATCUN-Gly Yield	BODIPY-ATCUN-Gly Yield
HATU	3%	25%	1%
PyBOP	10%	6%	1%
PFP/EDC	44%	31%	6%
PFP/EDC + Microwave	N/A	N/A	44%

The binding constants of ATCUN variants in solution form were determined using fluorescence spectroscopy. The interaction of Cu(II) ions with the ATCUN motif leads to fluorescence quenching, allowing for the calculation of binding constants.[41, 72] As shown in Table 3, the binding constants (K) for ATCUN-RhoB and ATCUN-FAM peptides highlight a significant difference in their affinity towards Cu(II) ions. ATCUN-RhoB showed a much higher binding constant (4.32×1012 M−1), corresponding to a log K of 12.64, compared to ATCUN-FAM's 2.10×109 M−1 with a log K of 9.32.[41, 141] This suggests that ATCUN-RhoB has a significantly stronger interaction with Cu(II) ions, which is crucial for effective sensing applications.

The structures of ATCUN-RhoB and ATCUN-FAM (Figure 9.B) are crucial in determining their binding efficiency. As depicted in Figure 9.B, ATCUN-RhoB includes a Rhodamine B moiety linked via a sarcosine spacer, while ATCUN-FAM incorporates a Fluorescein moiety. The presence of Rhodamine B, known for its high fluorescence quantum yield and photostability, enhances the peptide's ability to bind Cu(II) ions effectively. The ATCUN motif coordinates Cu(II) ions through a square planar geometry involving the N-terminal amine, histidine's imidazole, and backbone

amines.[142, 143] This strong interaction induces conformational changes that enhance fluorescence quenching, particularly in ATCUN-RhoB due to Rhodamine B's properties.[144, 145] The inclusion of sarcosine, a secondary amine, in the peptide sequence contributes to this efficiency by providing additional stabilization to the spirolactam ring of Rhodamine B, preventing its cyclization into a non-fluorescent form.[144] This stabilization ensures that the Rhodamine B remains in its open, fluorescent state, enhancing the peptide's ability to quench fluorescence upon metal-ion binding.[145, 146] The presence of sarcosine provides structural rigidity, which aids in maintaining the optimal orientation for metal-ion coordination. ATCUN-FAM lacks this stabilization mechanism, making it less stable compared to ATCUN-RhoB. The two hydroxyl groups in FAM can lead to the formation of various isomers and potential cyclization, reducing its binding efficiency and stability.

Table 3. Cu(II) and Ni(II) binding constants for ATCUN peptides determined by fluorescence or UV-Vis spectroscopy.

Peptide	Ion	K (mol/l)	logK
RhoB-Sar-ATCUN-Gly[41]	Cu^{2+}	4.32×10^{12}	12.64
FAM-ATCUN[44]	Cu^{2+}	2.10×10^{9}	9.32

As from previous studies, the selective binding of ATCUN-FAM was detected to CU(II) over NI^{2+} or Zn^{2+} at pH=6.5.[44, 147, 148] Paper I demonstrates the solution-based selectivity, Figure 10. A & B illustrate the selective binding of Cu(II) over Ni(II) at pH 6.5 using UV-Vis spectroscopy. The distinct absorbance peaks for Cu(II) complexes (Figure 10.A) and the pH-dependent binding profile (Figure 10.B) highlight the preference for Cu(II) under these conditions. As shown in Figure 10.B, at pH 6.5 a substantial increase in absorbance for Cu(II) indicates optimal binding

conditions due to formation of a square planar complex by ATCUN motif with Cu(II) ions.[41]

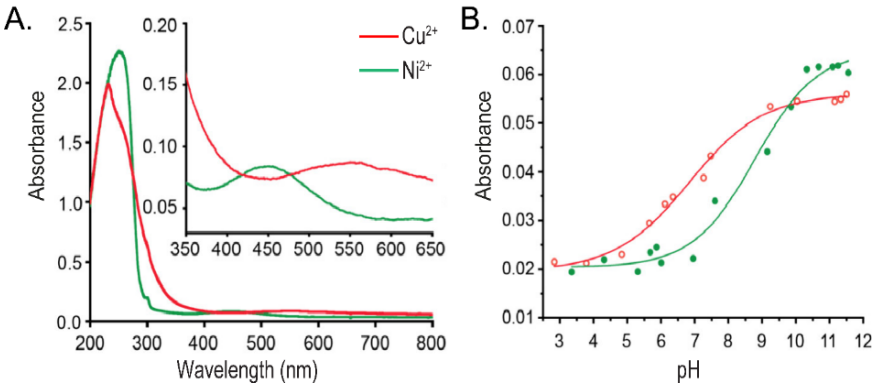

Figure 10: Results from Paper I that show selective binding of Cu^{2+} over Ni^{2+} at pH 6.5 using UV-Vis spectroscopy. (A) shows the absorbance spectra of Cu(II) and Ni (II) complexes with ATCUN peptides. The distinct peaks indicate a stronger interaction with Cu(II), especially in the visible yellow color at 500-565 nm range. (B) depicts the pH-dependent absorbance changes, highlighting optimal selective binding conditions for Cu(II) around pH 6.5, whereas Ni(II) shows increased binding at higher than 9.5 pH. Adapted from ACS Organic & Inorganic Au 2024, Volume 4, Issue 5, Hintzen, J. C. J.; Devrani, S.; Carrod, A. J.; Bayik, M. B.; Tietze, D.; Tietze, A. A., Fluorescence Labeling of Peptides: Finding the Optimal Protocol for Coupling Various Dyes to ATCUN-like Structures, with permission from ACS.

3.2 Mechanism of Selectivity

As explained in section 2.7, the ATCUN motif forms a highly stable square planar complex with Cu(II) via coordination of the N-terminal amine, two backbone amides, and the histidine side chain, conferring selectivity at physiological pH.[76] This specific arrangement is energetically favorable for Cu(II) due to its d9 electronic configuration that allows for optimal overlap between the metal's d-orbitals and the ligand's lone pairs, contributing to the high stability of the complex.[149] The specific pH of 6.5 ensures that the nitrogen atoms in the ATCUN motif are deprotonated and available for optimal coordination with Cu(II), enhancing selectivity over other ions like Ni(II). This has also been demonstrated at pH values lower than 10 and closer to physiological pH.[150, 151] Ni(II) and other competing ions, such as Co(II) and Mg(II), do not form similarly stable complexes at this pH.[150, 152] Specifically, Ni(II) tends to prefer octahedral coordination.[153, 154] As shown in Figure 10.B, pH values

lower than 9.65, such as 6.5, result in the complexation of Ni(II) with the ATCUN motif which is much less stable than Cu(II) ion, as indicated by lower absorbance values and supported by similar studies at physiological pH.[76]

Chapter 4

4.0 Automated Microfluidic Platform for High-throughput Biosensor Development (Paper II)

Paper II presents the Bio-Sensei platform, designed to streamline biosensor development by integrating microfluidics, electrochemical, and fluorescence measurements. It focuses on optimizing nanopore-based biosensors for detecting copper ions, incorporating machine learning for enhanced performance, and demonstrating high-throughput screening capabilities for biosensor applications.

4.1 Preceding Work

The results reported in the initial studies are the measured conductance versus Cu(II) concentration and fluorescence quenching versus Cu(II)/peptide ratio separately, each with a single sample repetition (N=1) as shown in Figure 11.A and Figure 11.B, respectively.[44, 64]

The S-shaped sigmoidal curves observed in these measurements are crucial for calibration in biosensors. Such curves represent binding interactions across concentration ranges, including threshold responses and saturation phenomena commonly observed in molecular recognition events.[155, 156] In our system, the curve represents the progressive occupation of ATCUN binding sites by Cu(II) ions, where the sigmoidal shape reflects the transition from minimal detection at low concentrations to signal saturation when all binding sites are occupied.[157, 158] This distinctive response profile enables precise quantification of Cu(II) concentrations within the nanopore sensor's dynamic range. The ATCUN peptide, labeled with a fluorescent marker (FAM), binds selectively with Cu(II), causing changes to conductance and fluorescence quenching,[159, 160] which is used as a measure of Cu(II) concentrations and Cu(II) to Peptide ratio, respectively.[157, 158] However, the two measurements - I-V and fluorescence - fall under distinct categories of electrochemical and spectroscopic methods, respectively. These methods utilize different measurement principles with distinct instrumental setups that require separate physical and analytical

workflows. This implies separate sample and assay preparation, measurement, data collection, and analysis. A notable difference in sample preparation is that the electrochemical readings were taken on ATCUN functionalized nanopore membrane samples, while the fluorescence readings were obtained on ATCUN sample solutions in bulk.

Due to these differences, the two measurements could not be taken for the same samples and at the same Cu(II) ion concentrations of the assay, hindering precise calibration and comprehensive analysis. This limitation restricted the statistical robustness of the data as it was not possible to obtain both measurements with repetition at the same concentrations.[161]

4.2 Transition to the Bio-Sensei Platform

The development of the automated, multiplexed platform marks a significant transition from traditional methods in biosensor research. This evolution highlights the integration of separate workflows—electrochemical and fluorescence measurements—into a unified system that enhances data collection and analysis. As described in Paper II,[162] the Bio-Sensei platform automates and synchronizes I-V and fluorescence measurements (Figure 11.C), allowing for multiplexed readings at the same Cu(II) concentration. This is demonstrated in the combined sigmoidal curve of conductance (N=6) and fluorescence quenching (N=3) as shown in Figure 11.D, significantly enhancing precision and reliability,[163] which is crucial to obtain accurate calibration based on the combined signal output for the biosensor.

The incorporation of Bio-Sensei offers numerous advantages such as it automates sample handling and data collection, reducing human error and increasing throughput. It enables simultaneous electrochemical and fluorescence measurements, providing comprehensive data at each concentration level.[164] The ability to collect more data points per experiment allows for detailed analysis

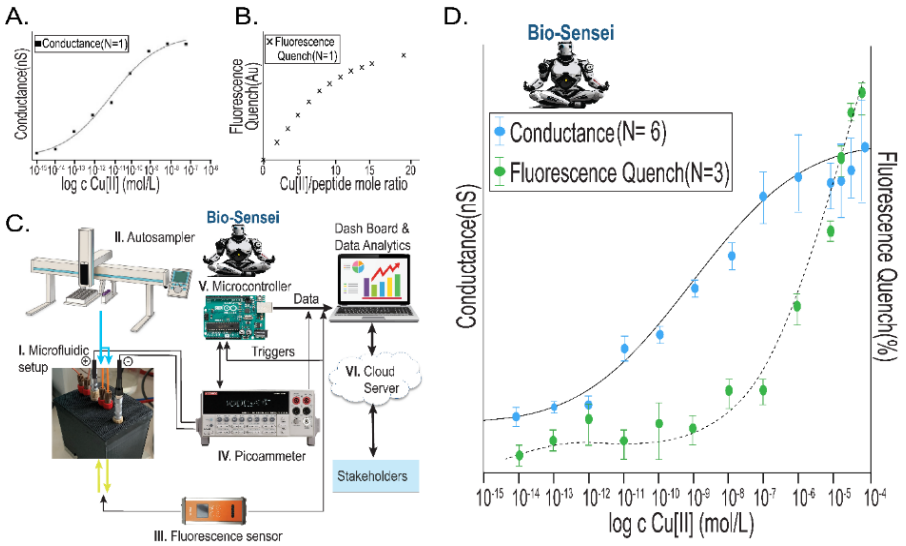

Figure 11: (A) Conductance vs. Cu(II) Concentration: This graph shows the relationship between conductance (in nano siemens, nS) and the logarithm of Cu(II) concentration (in mol/L). The curve is sigmoidal, indicating the binding interaction as the concentration of Cu(II) increases. (B) Fluorescence Quench vs. Cu(II)/Peptide Mole Ratio: This graph displays fluorescence quenching (in Absorbance units, AU) as a function of the Cu(II)/peptide mole ratio. The data suggests an increase in quenching with higher mole ratios, likely due to binding interactions. Adapted from Chemistry-A European Journal, 26 (39), Muller, L. K.; Duznovic, I.; Tietze, D.; Weber, W.; Ali, M.; Stein, V.; Ensinger, W.; Tietze, A. A., Ultrasensitive and Selective copper(II) Detection: Introducing a Bioinspired and Robust Sensor 2020, 8511-8517, with permission from Wiley. (C) Bio-Sensei System Setup: A schematic of the platform is shown, detailing various components: I. Microfluidic setup: The core component where samples are processed. II. Autosampler: Automates sample introduction into the system. III. Fluorescence Counter: Detects changes in fluorescence as part of the measurement process. IV. Picoammeter: Measures electrical signals generated by the biosensor. V. Microcontroller: Manages data collection and system operations. VI. Cloud Server: Facilitates data storage and analytics, allowing stakeholders to access the platform remotely via a dashboard. (D) Combined Conductance and Fluorescence Quench vs. Cu(II) Concentration: Bio-Sensei generated sigmoidal response of conductance and fluorescence quenching against the logarithm of Cu(II) concentration. Blue circles represent conductance measurements (N=6), while green circles indicate fluorescence quench measurements (N=3). Error bars suggest variability in measurements, with curves fitted to show trends in sensor response.

and better statistical validation, crucial for developing highly sensitive and selective sensors.[164] By integrating previously separate workflows into a single platform, Bio-Sensei streamlines experimental procedures and significantly reduces time and resource consumption compared to manual methods.[164] This facilitates precise calibration across different detection modalities and supports enhanced throughput screening necessary for developing next-generation biosensors.[165] The sigmoidal nature of the curves is better calibrated using Bio-Sensei due to its

multiplexed measurements(Figure 11.C). By enabling synchronized data collection at identical Cu(II) concentrations, it is possible to perform comprehensive analyses, crucial for developing sensors with high sensitivity and selectivity.[161, 166] This capability not only accelerates sensor development but also enhances the accuracy and reliability of analytical results.[161, 166]

Table 4 presents a comparison of calibration metrics between the Bio-Sensei platform and traditional setup methods. Bio-Sensei provides specific sensitivity values for both fluorescence quenching and conductance, offering a comprehensive understanding of the sensor's performance across different concentration ranges. In contrast, studies using traditional methods show LOD only for fluorescence quenching, and along a narrow sensitivity range.[44, 64] Furthermore, traditional methods don't report bias, limiting insight into the measurement accuracy of the biosensor. The analysis performed on the Bio-Sensei platform provides average sensitivity and bias for both fluorescence quenching and conductance, indicating potential systematic errors in measurements, which is crucial for refining sensor accuracy. It also helps to compute the biosensor's LOD values, highlighting its ability to test extremely low concentrations across a much wider sensitivity range.

The transition from traditional methods to the Bio-Sensei platform represents an advancement in biosensor development capabilities. By integrating automation and multiplexing capabilities, it's possible to explore the potential of biosensors more effectively, ensuring robust testing and reliable results across various applications.[155, 163] By utilizing sigmoidal models for both I-V and fluorescence data, the platform achieves high sensitivity across a uniform yet broad concentration range, from femtomolar to micromolar levels. The platform possesses the ability to provide detailed calibration metrics such as sensitivity, bias, LOD, etc. across multiple measurements which is critical for developing robust biosensors.

Table 4. Calibration Metrics for Bio-Sensei Platform against the Tradition measurement setups of I-V measurement cell and Confocal Laser Scanning Microscopy (CLSM)

	Calibration on Bio-Sensei (Paper II)		**Calibration using traditional I-V measurement cell and CLSM**[44, 64]	
	Fluorescence Quenching	**Conductance**	**Fluorescence Quenching**	**Conductance**
Avg. Sensitivity	1.86 %/Log(M)	273.9 nS/Log(M)	-	-
Most Sensitive Range	10^{-7}-10^{-4} M	10^{-12}-10^{-8} M	10^{-6} - 10^{-4} M	-
Bias	-3.14 %	-1277 nS	-	-
LOD	10^{-6} M	10^{-15} M	13.5 X 10^{-9} M	-

4.3 ATCUN Functionalization on Nanopore membranes

Previous reported studies used Ion-track etched nanopore membranes that were obtained from the GSI in Darmstadt, Germany.[44, 167] In this study, commercially available membranes were used from ip4it for grafting peptides to the nanopores.

In the proposed biosensor, ATCUN peptide is the bioreceptor that is functionalized on nanopore membranes which acts as the biocompatible layer to the bioreceptor (as discussed in section 2.2 and Figure 2). Initially, nanopore membranes are functionalized by incorporation of the COOH-groups. These carboxyl groups were generated following alkaline hydrolysis of PET esters during the track etching process where exposure of the PET surface to NaOH selectively etches ion-irradiated regions to create nanochannels while generating terminal carboxylate groups on the polymer

surface. These surface-bound carboxyl groups undergo activation via a carbodiimide-mediated reaction using EDC and PFP in ethanol, forming highly reactive Pentafluorophenyl esters. The activated membrane is subsequently treated with ethylenediamine (EDA), which covalently couples to the esters through nucleophilic substitution, introducing primary amine functionalities as shown in Figure 12.A.

For ATCUN-dye conjugation, the peptide's N-terminal amine reacts with the activated carboxylic acid group of the fluorophore using HATU as the coupling agent as shown in Figure 12.B. This reaction occurs in DMF with N,N-diisopropylethylamine (DIPEA) as a base, facilitating the formation of amide bonds through HATU's uronium-based activation mechanism. The procedure follows established protocols for carbodiimide chemistry and modern peptide coupling techniques.[41, 168]

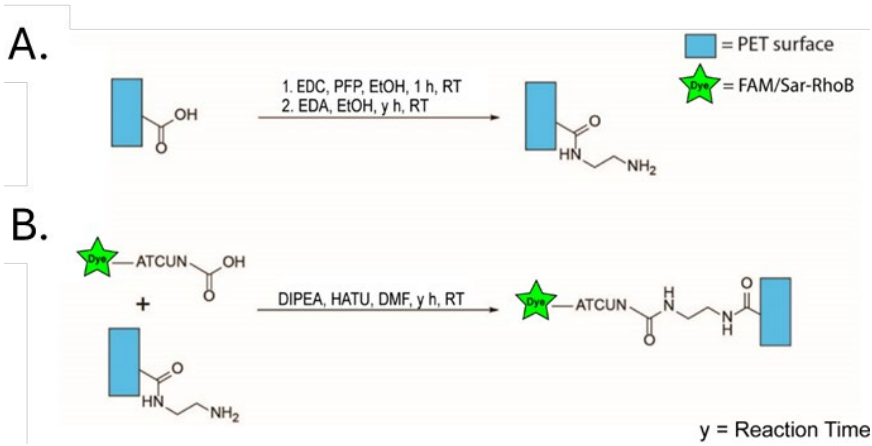

Figure 12: (A) Schematic of the chemical functionalization process on a PET surface. The PET surface is first activated with EDC and PFP in ethanol for 1 hour at room temperature, followed by reaction with EDA in ethanol for a specified reaction time (y hours). (B) Further functionalization with ATCUN peptide using DIPEA and HATU in DMF for a specified reaction time (y hours) at room temperature.

4.4 Nanopore-based Selectivity towards divalent ions

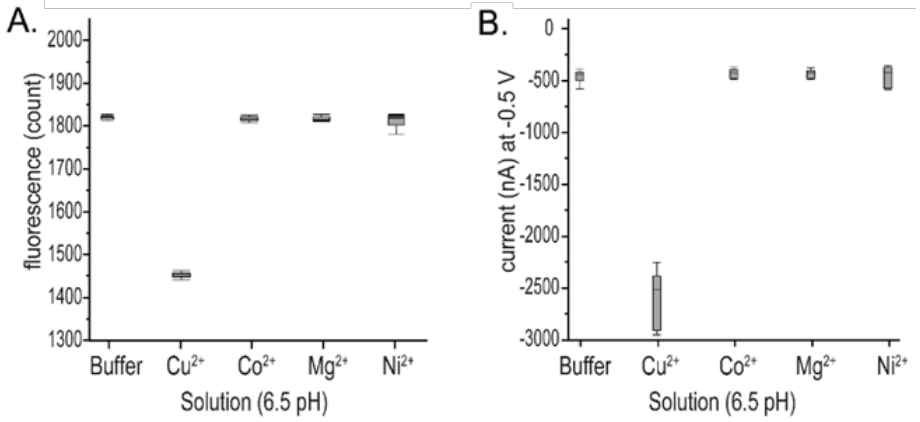

Figure 13: Results from Paper II that show selective binding of Cu^{2+} over other metal ions at pH 6.5 using the Bio-Sensei platform. (A) presents fluorescence counts showing significant quenching only in the presence of Cu^{2+}, indicating selective binding. Other ions like Co^{2+}, Mg^{2+}, and Ni^{2+} do not significantly affect fluorescence. (B) shows current measurements at -0.5 V, where Cu^{2+} causes a marked decrease in current, unlike other ions, confirming selective electrochemical response.

In Paper II,[162] the selectivity of ATCUN-functionalized nanopore membranes was tested against a range of other ions using multiplexed fluorescence and I-V measurements on the Bio-Sensei platform. This approach validated the biosensor's practical applicability by using a broader set of competing metal ions beyond Cu(II) and Ni(II). Figure 13.A shows the fluorescence quenching as the fluorescence signal significantly decreases in the presence of Cu(II) due to quenching upon binding. Other ions do not cause similar quenching, indicating minimal interaction as has also been indicated in another study.[169]

Similarly, Figure 13.B presents the I-V Measurements where the current changes dramatically only with Cu(II) ions, confirming selective electrochemical response. Statistical analysis using t-ratios and p-values further supported the biosensor's response to selected ions as shown in Table 5. High t-ratios and low p-values (<0.0001) for Cu(II) in both multiplexed readings indicate significant selectivity compared to buffer conditions, the significance of such values is well established.[170, 171]

The selectivity coefficient parameter quantifies the biosensor's preference for Cu(II) over other ions, with lower K values for non-target ions confirming minimal interference,[172] which implies both fluorescence and I-V measurements. Cross-reactivity percentages are used to assess how much the sensor's response to non-target ions mimicked its response to Cu(II).[173] Low cross-reactivity percentages indicates high specificity to Cu(II), minimizing false positives from other ions.[174, 175] These parameters collectively validate the biosensor's ability to selectively detect Cu(II) ions with high accuracy and minimal interference from other metal ions, enhancing its reliability in practical applications. The selective nature of ATCUN motifs for Cu(II) ions at pH 6.5 in solution based and nanopore-functionalized form are highlighted in Paper I,[41] and II.[162] Several preceding studies have also highlighted the ability of ATCUN motif for Cu(II) ion detection.[44, 147, 148]

Table 5. Summary of the M2+ selectivity analysis in comparison to response in buffer of the nanopore-based biosensor from multiplexed fluorescence (Fluor.) and I-V measurements (Paper II)

	Cu^{2+} to buffer		**Co^{2+} to buffer**		**Mg^{2+} to buffer**		**Ni^{2+} to buffer**	
	Fluor.	**I-V**	**Fluor.**	**I-V**	**Fluor.**	**I-V**	**Fluor.**	**I-V**
|t -Ratio|	110	53	1.1	0.7	0.7	0.7	1.8	0.1
Prob > |t|	<.0001	<.0001	0.27	0.5	0.5	0.5	0.07	0.9
Selectivity Coefficient (K)	-	-	0.01	0.18	0.01	0.18	0.02	0.18
Cross Reactivity	-	-	1%	17.6%	0.66%	17.6%	1.7%	18.5%

4.5 IV / Fluorescence – Based Models for Cu(II) Prediction

Following the evaluation of the nanopore-based biosensor's stability, selectivity, and sensitivity using the Bio-Sensei platform, the focus shifts to the data analysis methodologies employed for accurate Cu(II) concentration prediction. The primary objective was to calibrate the sensor signal dependence against known analyte concentrations, enabling the development of predictive models for unknown sample concentrations. This section details the progression from initial data processing and signal correction, through the application of traditional I-V and fluorescence-based models and culminating in the implementation of supervised machine learning algorithms to enhance prediction accuracy and reliability.

As explained in section 2.8 and Figure 6, sigmoidal models provide a comprehensive representation of sensor response across a wide range of analyte concentrations. These capture the initial lag phase, the linear dynamic range, and the saturation phase, offering a more detailed understanding of sensor behavior.[176] They enhance sensitivity in the mid-range concentrations where changes are most detectable, with steep slope in this region allows for precise detection and differentiation between small changes in analyte concentration.[176] The non-linear nature of sigmoidal curves provides superior fitting to experimental datasets from multiple sensors, significantly reducing errors associated with linear approximations in automated analysis pipelines. This mathematical robustness enables more reliable calibration and prediction models when processing data from numerous sensing elements simultaneously, particularly at extreme concentration values where linear models typically fail.[92]

Initial efforts to correlate the sensor signal with Cu(II) concentration in 6.5 pH buffer involved analyzing the individual fluorescence and

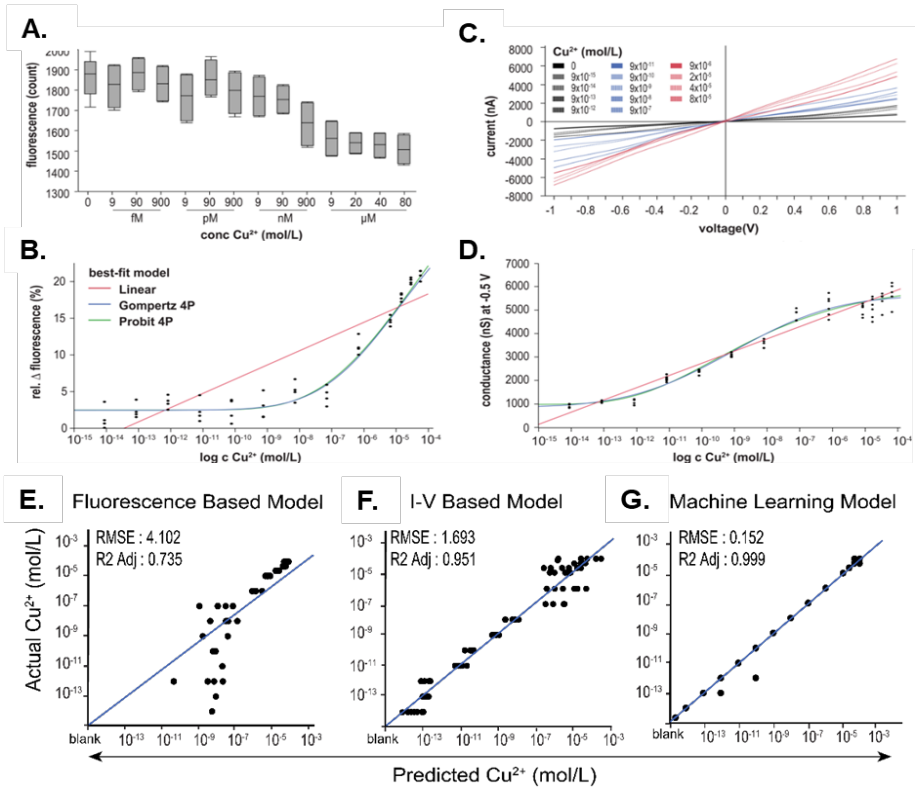

Figure 14: Selectivity of the nanopore-based biosensor (0.03 µm pore size, 5 x 10^5 pores, MES/KCl buffer 100 mM, pH 6.5) (A) fluorescence in buffer (N = 52) with increasing concentrations of Cu(II) in 6.5 pH buffer (N = 4). (B) comparison of best-fit models (linear, Gompertz 4P and Probit 4P) for the fluorescence data. (C) current vs. voltage diagram reported for 6.5 pH buffer (N = 78) and increasing concentrations of Cu(II) in buffer(N = 6). (D) Conductance for each reported Cu(II) concentrations at -0.5 V and comparison of best-fit models (linear, Gompertz 4P and Probit 4P) for the I-V data. Performance of Actuat vs. (E) Fluorescence based logistic model. (F) I-V (conductance at -0.5 V) based logistic model. (G) Machine Learning (Boosted Neural Network) model that combines input features derived collectively from fluorescence and I-V measurements. Adapted from Advanced Sensor Research, 4, Devrani, S.; Tietze, D; Tietze, A. A., Automated Microfluidic Platform for High-Throughput Biosensor Development, (2400116) with permission from Wiley.

conductance (I-V) responses. The fluorescence signal show a gradual decrease as Cu(II) concentration increases, particularly in the higher nano- to micromolar range (Figure 14.A), consistent with Cu(II)-induced fluorescence quenching. To address potential membrane denaturation effects, the relative change in fluorescence (rel. Δ fluorescence) is calculated and plotted against increasing Cu(II) concentrations on a logarithmic scale as shown in Figure

14.B. This adjustment reveals higher variance at lower Cu(II) concentrations, impacting model accuracy within this range.

Complementary to fluorescence, the observed I-V curves show increasing slopes as the Cu(II) concentration increases (Figure 14.C). Specifically, conductance values calculated at -0.5 V exhibit a sigmoidal relationship with Cu(II) concentration in log scale as shown in Figure 14.D, which is consistent with prior findings alluded to in section 4.1, Figure 11.D and Paper II.[162] Regression models based on sigmoidal fits are then applied to both fluorescence and I-V data, reflecting standard practices in biosensor analysis.

Despite their utility, models based solely on fluorescence or I-V data demonstrated limitations in accuracy across the entire concentration range. As illustrated in Figures 14.A,B the fluorescence-based model shows higher prediction accuracy at higher Cu(II) concentrations but struggle at lower concentrations due to higher variance. Conversely as shown in Figure 14.C,D the I-V model achieves superior accuracy at lower concentrations but plateau at higher ranges with lower error and higher prediction accuracy at lower concentrations, contrary to the fluorescence model which displays greater accuracy at higher concentrations. These complementary strengths and weaknesses underscored the need for a more advanced approach to leverage the combined data from both sensing modalities for improved prediction accuracy. This motivated the integration of machine learning algorithms, which are designed to handle complex and non-linear relationships, to achieve robust predictions across the full range of Cu(II) concentrations.

4.6 Impact of Machine Learning

The standard practice for machine learning implementation in this thesis involves capturing data from the Bio-Sensei platform's hardware layer for ATCUN functionalized nanopore membranes. This data passes through a data analytics pipeline in the software

layer, where signal processing and feature engineering are applied to prepare it for supervised machine learning algorithms.[162] Typically, the data is split into training, validation, and test sets as 60%, 15%, and 25%, respectively and the model is trained to classify Cu(II) concentration in buffer.

The ability of machine learning models to handle complex, multiparameter data has been established in medical applications, where various algorithms including extreme gradient boosting, random forest, neural networks, and logistic regression have been successfully applied to predict breast cancer diagnosis delays.[177] As shown in prediction vs output plots of Figure 14.G, machine learning models based on the combined features captured from the I-V and fluorescence measurements, outperform individual sigmoidal models based solely on each of the measurement principles(See Figure 14.E,F). This approach offers an elegant method to build models to predict Cu(II) concentration performed on the biosensor.

The three best performing algorithms are shown in Table 6 from Paper II,[162] these are identified for further consideration based on its potential in performance, scalability and practical utility in the proposed biosensor.[178]

The brief evaluation of Table 6 shows the performance results of several of the discussed algorithms on test set post processing. The Decision Tree performs the best with a perfect Receiver-Operator Area under Curve (ROAUC) score indicating no misclassification with high accuracy as well as low error along with an excellent fit. This high accuracy is consistent with the performance of decision tree models in other classification tasks, where they have shown excellent results in multiclass classification problems.[179] The low misclassification rate suggests that the model is capable of accurately categorizing different concentration levels, similar to how decision trees have been successfully applied in classifying various types of data with high precision.[180] While known for their

adaptability, Decision Trees can overfit complex datasets.[181,182, 183] In this case, they report a tendency towards overfitting as multiple splits ranging up to 31 are observed which severely limits its utility especially when large datasets need to be trained.

Table 6. The performance results of the three best machine learning models for the test set.

Method	Set	N	Misclassification Rate	ROAUC	RASE	R^2
Decision Tree	Test	4745	0.000	1.000	0.004	1.000
Neural Boosted	Test	4745	0.007	0.999	0.090	0.995
Nominal Logistic	Test	4745	0.137	0.978	0.339	0.945

Boosted Neural Network demonstrates a near-perfect classification and slightly higher error rates than Decision Tree but still low in value. Further, a generalized R^2 value of 0.995 indicates its robust performance. It demonstrates strong performance with a low misclassification rate, suggesting its robustness in handling diverse concentration profiles. This is consistent with the performance of neural networks in other complex classification tasks, such as mosquito species detection, where deep convolutional neural networks have achieved high average accuracies of 97.7%.[184] Nominal Logistic Fit present metrics that suggest good performance but lower than the other models presented in Table 6. Their performance is also indicative of similarity in approach to conductivity or fluorescence based sigmoidal modelling done in section 4.5. Logistic Models, while useful, report lower performance and scalability compared to neural networks as shown in multiple studies.[185-187]

4.6.1 Rationale for Selecting Neural Networks

Neural networks are favored for their ability to manage complex data relationships,[188,189] which is crucial for biosensors dealing with diverse input features derived from multiplexed I-V and fluorescence readings. They have also been shown to adapt to various conditions and improve generalization performance when trained on diverse datasets.[190] Further they offer scalability when expanded with more layers or nodes to improve performance as more data becomes available,[191] which allows neural networks to handle increasingly complex tasks and larger datasets, making them suitable for a wide range of applications.[192] A study on acute stroke outcome prediction, the generalized regression neural network model showed better performance based on sensitivity, specificity, and accuracy compared to logistic regression.[186] Similarly, in predicting dry eye disease after vitrectomy, artificial neural networks consistently outperformed the logistic regression model in terms of predictive power.[185] Their robustness and adaptability prevent overfitting while allowing for scalability with additional data, making them ideal for real-world applications with high data variability and large datasets.[190, 193] These factors favored neural networks as the ideal choice as they were expected to maintain high prediction accuracy across diverse concentration ranges, making them ideal for biosensor applications in detecting Cu(II) ions in human serum.

Chapter 5

5.0 Multimodal Microfluidic Biosensor with Neural Network Analytics for Accurate Detection of Cu(II) in Human Serum (Paper III)

Paper III presents a method for detecting copper ions in human serum by integrating multimodal microfluidics with neural networks. The study addresses limitations of traditional methods and proposes a solution for improved diagnosis and monitoring of copper-related disorders.

5.1 Design Consideration in Microfluidic Systems

Microfluidics enhances biosensor sensitivity and specificity by controlling fluid dynamics at the microscale.[194, 195] Its relevance to automated platforms and POC devices for medical diagnostics and environmental monitoring are discussed in section 2.9.1.

For microfluidics design, the choice of materials and flow path configurations has significantly shown to impact the performance and reliability of such devices.[196, 197] For instance, such factors can influence fluid transport efficiency by minimizing dead volumes to improve the overall functionality of microfluidic systems,[197] and the configuration of flow paths determines the chip architecture, directly affecting the performance of microfluidic biochips.[198] In biochips with electrochemical cells, electrode design is crucial as it directly influences the surface area exposed to the electrolyte, which governs the density of active sites and defect density—structural imperfections such as voids or grain boundaries that arise during fabrication. Unequal electrode masses create asymmetrical surface areas, leading to heterogeneous charge distribution and preferential ion flow pathways.[199] For example, electrodes with higher mass exhibit greater surface roughness and defect density due to uneven electrodeposition, which alters local electrochemical kinetics and electric double-layer (EDL) dynamics.[199-202] These defects, modulated by electrode volume and deposition parameters

(e.g., voltage, duration),[203,204] disrupt ion transport uniformity, causing rectification effects in current-voltage (I-V) profiles and reducing measurement accuracy.[204,205] Thus, optimizing electrode symmetry and defect density through controlled manufacturing processes is critical for achieving linear, reproducible electrochemical responses in microfluidic biosensors.

5.1.1 Glass-Based vs. PMMA-Based Microfluidics

The Bio-Sensei platform in Paper II integrated a vendor made glass-based microfluidic system (procured from Mesobiotech©),[162] with electrochemical and fluorescence measurement capabilities (Figure 11.C,D) to facilitate high-throughput biosensor screening. It utilized a simpler flow path with top and bottom fluid channels in parallel (Figure 15.A and Figure 16.A), which were not particularly designed to provide the favorable fluid flow dynamics. This often results in bubble formation and had to be counteracted by higher flows. Further, inconsistent Au electrode surface areas on either side of the chips (Figure 15.B) with unequal thickness formed due to unstandardized gold deposition on either side of the electrochemical cell. The cumulative effect of factors such as flow inconsistencies, unequal mass configuration that altered charge distribution, and electrochemical kinetics led to rectification in the calibrated I-V curves. Previous literature confirms that rectification behavior is defined by specific directional preference for ion transport that results in a non-linear (cubic fit) I-V calibration curve (as shown in Figure 16.B).[206] Further, such glass-based designs are prone to breaking and leakage, they are not feasible for usage to a design with several moving parts such as the one proposed here to

maintain the reconfigurability of the microfluidics to test more than one sample membrane.

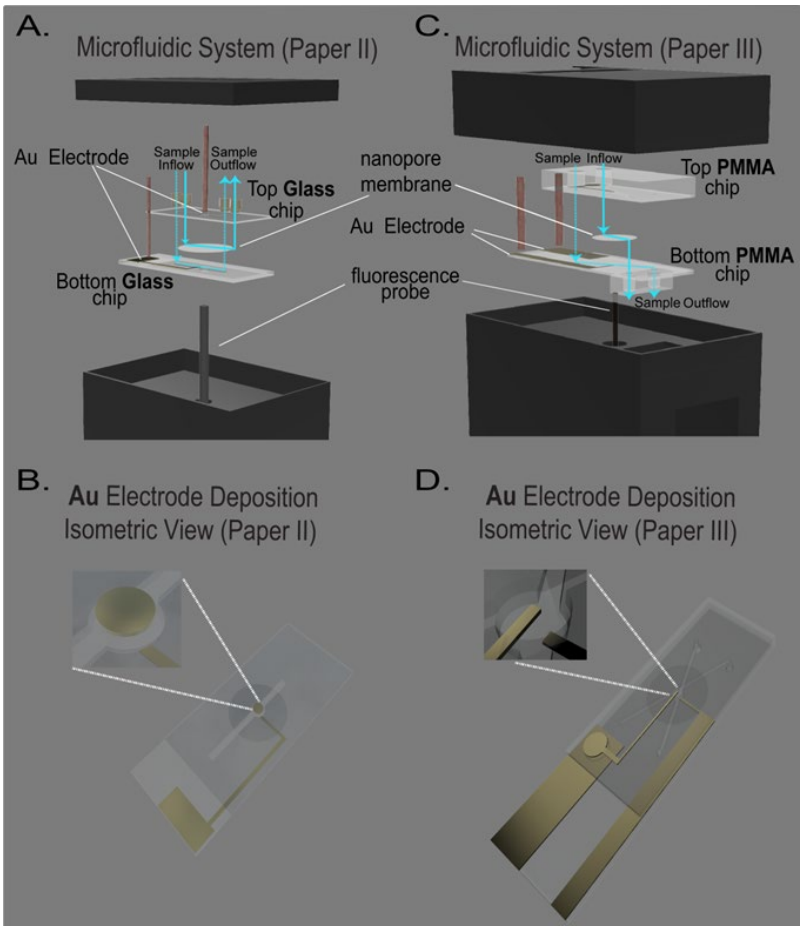

Figure 15: (A) Microfluidic system design from Paper II, illustrating the integration of Au electrodes on a glass chip with sample inflow and outflow (in blue) channels for fluid handling. (B) Isometric view of the Au electrode deposition on the glass chip (from Paper II) with inconsistencies in surface area due to unequal mass configurations which can be observed by difference in patterns of the top and bottom Au electrode patterns. (C) Microfluidic system design from Paper III, featuring a nanopore membrane integrated with Au electrodes on PMMA chips for enhanced functionality. (D) Shows an isometric view of the Au electrode deposition on the PMMA chip (from Paper III) with even mass configurations, ensuring symmetry in surface area and defect density, this can be observed by similarity in top and bottom Au electrode deposition patterns.

In contrast, Paper III presents an in-house fabricated reconfigurable electro-fluorochemical microfluidic cell (Figure 15.C), that provided robustness and reduced the risk of breakage compared to glass-based microfluidics used previously in Paper II. This PMMA-based microfluidic cell is designed to sustain pressures up to 105.17 kPa

(calculated in Paper III), ensuring reliable operation under typical microfluidic conditions owing to the material's low brittleness and high tensile strength which has long been established previously.[207-209] The flow paths are designed to cross and intersect at the center of the microfluidics where the measurements are taken (Figure 16.C). This ensures no invasive mass transfer between the two channels until their intended mixing at the intersection. This also provides a more complex flow profile and controlled mixing of the fluid inflow on either side of the electro-fluorochemical cell that leads to promoting a more even distribution and interaction of the sample. Further the gold electrodes on either side of the electrochemical cell are deposited to have even mass configuration (as shown in Figure 15.D) which creates symmetry in surface area, defect density, and overall electrode structure and hence avoids potential rectification due to electrode characteristics.

The high Peclet numbers as reported in Paper III indicated efficient analyte transport to the sensor surface, enhancing the sensor's performance by maintaining a higher local concentration of the analyte. The significance of this metric in sensor design has been already established.[206] This design results in a linear calibration I-V curve (Figure 16.D), indicating a more predictable and consistent response that improved precision, reliability in measurements and symmetry of ion flow in both directions.

5.1.2 Impact on Detection Accuracy

The transition from Paper II's glass-based microfluidic system to Paper III's PMMA design enhances durability and reconfigurability.[208, 210] This change contributes to a more linear calibration curve (Figure 16.D), improving the predictability and consistency of Cu(II) detection. This implies that the microfluidic system in Paper III offers enhanced sensitivity and accuracy for Cu(II) detection, which is crucial for precise quantification. The sixfold increase in N (number of repetitions) value from Paper II

(Figure 16.B) to Paper III (Figure 16.D) indicates more repetitions of current measurements at each voltage, reflecting enhanced stability and repeatability in the new design. The symmetry about the y-axis

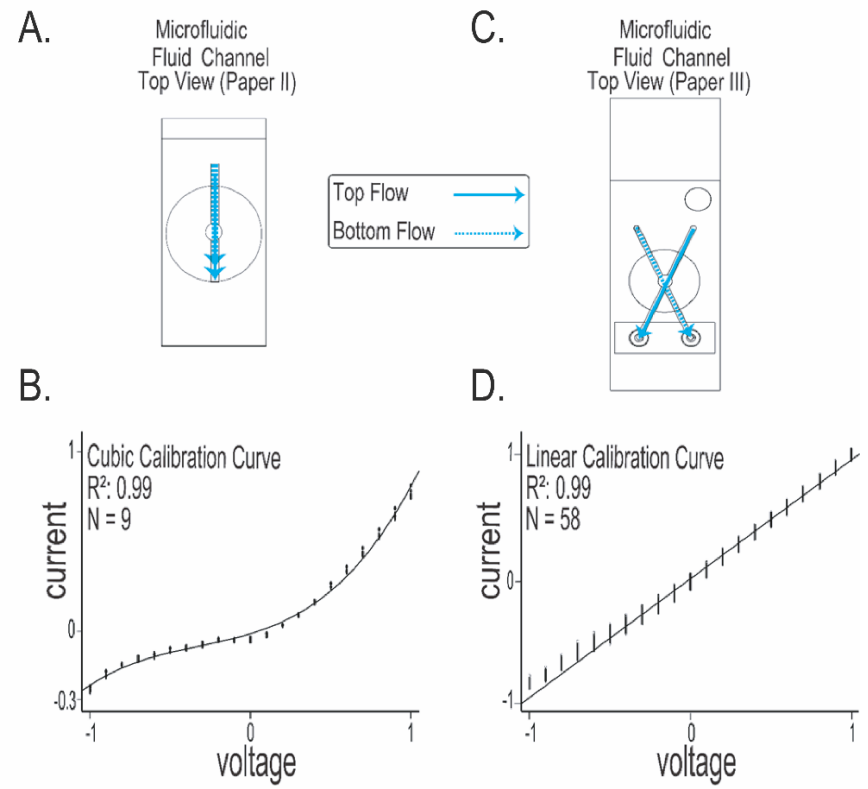

Figure 16: Microfluidic Pathway (Top view): The sample fluid channels with the flow on top (solid blue line) and bottom (dashed blue line) of the sample membrane. (A) Paper II microfluidics utilizes a simpler flow path with top and bottom channel flows in parallel. (B) Corresponding cubic calibration curve for current vs. voltage with an R^2 value of 0.99, based on 9 repetitions (N = 9). (C) Schematic of the microfluidic fluid channel design from Paper III, showing intersecting flow path that cross at the center to promot even flow distribution and interaction of the sample. (D) Corresponding linear calibration curve for current vs. voltage with an R^2 value of 0.99, based on 58 repetitions (N = 58). The transition of the cubic (Paper II microfluidics) to a linear calibration curve in Paper III implies improved accuracy and reliability in Cu(II) detection, with increased N(repetitions) values reflecting enhanced measurement stability, the improved design in Paper III utilizes a reconfigurable pathway that supports a more efficient flow, reducing rectification and leading to a symmetric calibration curve about the y-axis, indicating balanced sensor responses.

(linear calibration curve) represents a balanced system with reduced variability and no rectification, which is crucial for minimizing distortion so that clearer and more reliable data interpretation can be provided. The use of PMMA in Paper III offers robustness and reconfigurability compared to glass in Paper II,

reducing breakage risk and allowing for more flexible integration with other components leading to increased repetitions as has also been demonstrated elsewhere.[207, 208, 210] Overall, this significantly improves the durability and adaptability of the electro-fluorochemical cell that is integrated at the core of the Bio-Sensei platform.

5.2 Determination of ATCUN-Fluorophore response

ATCUN-RhoB and ATCUN-FAM functionalized nanopore are compared in their performance for detection of Cu(II) ions. Based on this, the intent is to reveal significant insights into their structural and functional differences (Figure 17.A), as well as their application in biosensing.[72, 141]

After membranes were functionalized with both ATCUN-FAM and ATCUN-RhoB peptide (as per section 4.3), IV curves are recorded by applying a voltage in the range of -1 to +1. Figure 17.B presents a typical normalized current-voltage (I-V) curve highlighting regions of positive and negative conductance and remanence. The shaded area under the curve represents the overall electrical performance of the peptides, indicating how structural differences influence conductance. Similar approaches have been applied in analyzing the electrical properties of various materials, including photovoltaic modules and semiconductive peptides.[211, 212] The PCA biplot (Figure 17.C) demonstrates that ATCUN-RhoB excels in both

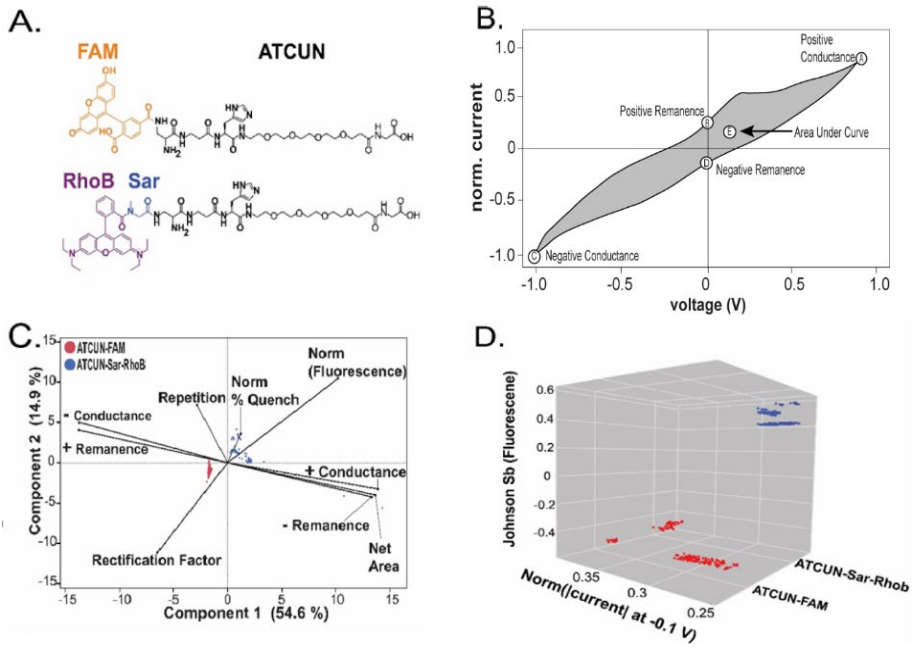

Figure 17: (A) Structural Representation of Peptides: The figure illustrates the chemical structures of two peptides, ATCUN-FAM and ATCUN-Sar-RhoB. ATCUN-FAM features a fluorescein moiety, while ATCUN-Sar-RhoB includes a Rhodamine B moiety linked via sarcosine. The structural differences significantly influence their binding efficiency and fluorescence properties. (B) Normalized Current-Voltage (I-V) Curve: This plot displays the normalized current as a function of voltage, highlighting regions of positive and negative conductance and remanence. The shaded area under the curve represents the overall electrical performance of the peptides in terms of conductance. (C) Principal Component Analysis (PCA) Biplot: The PCA biplot compares the performance of ATCUN-FAM (red dots) and ATCUN-Sar-RhoB (blue dots) based on various parameters derived from I-V and fluorescence measurements. Vectors indicate the direction and magnitude of features such as conductance, remanence, rectification factor, and normalized fluorescence. (D) 3D Scatter Plot of Normalized Current and Fluorescence: This plot shows the relationship between normalized current at -0.1 V and fluorescence (Johnson Sb), illustrating a clear separation between ATCUN-FAM (red points) and ATCUN-Sar-RhoB (blue points). The distinct clustering indicates differences in their electrical and fluorescence properties.

fluorescence quenching and electrical conductance. It shows that ATCUN-RhoB clusters closely with vectors indicating high normalized fluorescence and quenching efficiency. This suggests robust fluorescence quenching capabilities, making it suitable for applications requiring high sensitivity.[41, 44, 145]

The electrical performance of ATCUN-RhoB is also notable; its clustering with positive conductance vectors indicates enhanced electron transfer processes. The strong binding affinity of Cu(II) ions to the ATCUN motif likely facilitates electron transfer, enhancing

electrical conductance.[44] The separation between ATCUN-RhoB and ATCUN-FAM highlights their distinct functional properties. This is supported by the structural stability provided by Rhodamine B, which maintains the peptide's active conformation during ion interaction (Figure 17.A).[144, 213] Reinstating their performance, Figure 17.D presents the 3D scatter plot that further distinguishes these peptides based on normalized current and fluorescence, reinforcing the superior performance of ATCUN-RhoB in terms of fluorescence intensity.[145, 214]

5.3 Detection in Human Serum

Paper III further utilizes neural networks for predicting Cu(II) concentrations in human serum (HS) with Bio-Sensei Platform's multiplexed I-V and fluorescence measurements, which capture comprehensive data indicative of Cu(II) binding to ATCUN-functionalized membranes. This approach aligns with prior demonstrations of machine learning-enhanced multiplexed sensing platforms.[163, 215] While the platform collects data across Cu(II) concentrations in HS, individual features such as %Quench (Figure 18.A) and current at -0.5 V (Figure 18.B) plateau at higher concentrations, limiting their predictive utility. Fluorescence quenching saturates as ATCUN binding sites on nanopores become fully occupied, whereas I-V responses plateau due to maximal compression of the Electric Double Layer (EDL) (as explained in

section 2.3), where additional Cu(II) binding no longer alters ion transport dynamics despite increasing analyte levels.

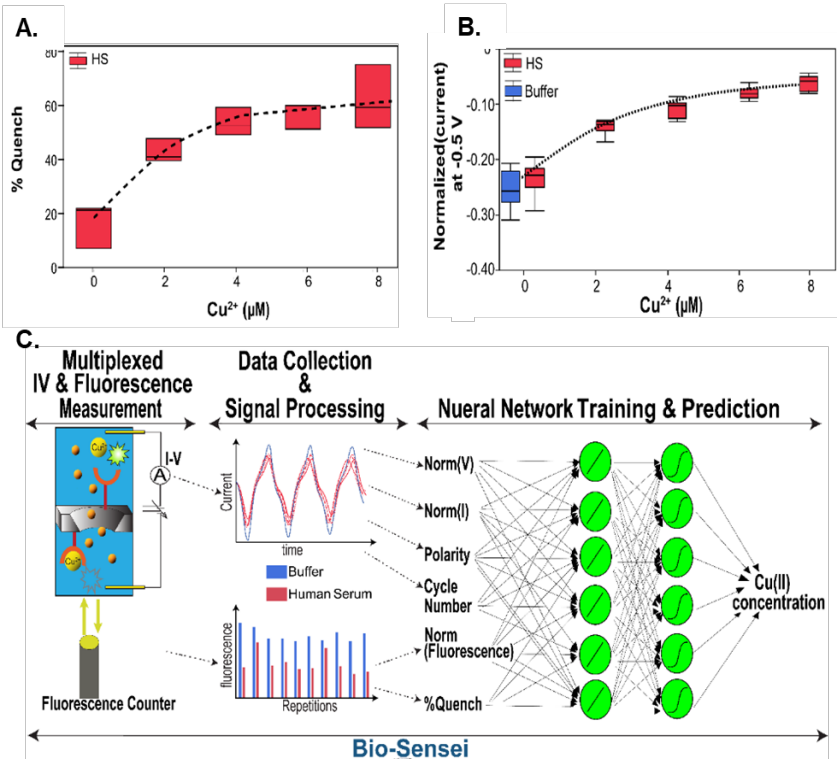

Figure 18: Sensitivity analysis of the ATCUN-RhoB functionalized nanopore membrane on the Bio-Sensei platform with various copper (Cu(II)) concentrations in HS (human serum) and interim buffer washes. (A) Percentage quench of fluorescence(N=3) in Cu(II)-HS solutions, indicating the degree of reduction in fluorescence as it reaches saturation with increasing Cu(II) concentration. (B) Box plot of normalised current (between -1 to 1) at -0.5 V for different Cu(II)concentrations in buffer(N=100) and HS(N=10), showing the saturation (plateau) effect at higher concentrations. (C) Methodology of the Bio-Sensei platform for Cu(II) detection in human serum via multiplexed I-V and fluorescence measurements. Cu(II) binding to ATCUN-functionalized membranes alters its electrical and fluorescence (optical) properties, producing features such as normalized current, voltage, polarity, fluorescence quenching, and cycle number. These features are fed as input into a multilayer perceptron (MLP) neural network, which processes complex interactions to predict Cu(II) concentrations with improved precision and reliability. This approach outperforms individual signal-based models by utilizing combined data for enhanced prediction accuracy.

5.3.1 Multilayer Perceptron Based Prediction

To improve performance, feature engineering is expanded to include more descriptive features as inputs to the Multilayer Perceptron (MLP) which is a feed forward neural network. In this regard, features extracted are normalized voltage, normalized

current, polarity, cycle number from I-V and normalized(fluorescence), % quench from fluorescence measurements (Figure 18.C). Here, polarity indicates the direction of applied voltage, and the cycle number is a running count of the cycles in the I-V waveform. Further, % quench quantifies the reduction in fluorescence intensity. By analyzing these combined features, MLP can identify patterns that are not apparent when considering single features derived from IV or fluorescence data alone, as has been previously reported aswell.[178, 215] This enhances classification accuracy by using the full spectrum of data to predict Cu(II) concentrations, even when individual measurements plateau.[178] The neural network model processes complex interactions between variables or input features, allowing it to maintain sensitivity and accuracy across a wider range of concentrations. This approach ensures reliable detection even when traditional methods face limitations due to signal saturation (Figure 18.A,B), which has also been reported previously.[215,216,217] By analyzing these features together, MLP can extract more nuanced patterns that are not apparent when examining each feature in isolation.[182, 183] The metrics presented in Table 7 further validate the robustness and accuracy of the MLP classifier from Paper III on the test set. The high Generalized R^2 and Entropy R^2 values indicate that the model explains a significant portion of the variance in the data.[218] The low RASE and Mean Absolute Deviation values suggest minimal prediction errors, while the low Misclassification Rate confirms the model's high accuracy.[218, 219] The -LogLikelihood value provides a measure of the model's fit, with lower values indicating better fit.[219] This analysis underscores the potential of neural network models to enhance the accuracy and reliability of Bio-Sensei in complex biological sample analyses. Table 7 (along with results in Paper III) highlights the MLP classifier's strengths and areas for improvement to enhance Bio-Sensei's accuracy and reliability in complex biological sample

analyses, their utility has also been independently verified for similar studies.[218, 220-224]

Table 7. Performance Metrics of Multilayer Perceptron Classifier on Test Set

Measures	Value
Generalized R^2	0.997
Entropy R^2	0.980
RASE	0.104
Mean Absence Dev	0.022
Misclassification Rate	0.018
-LogLikelihood	200.070
N	6413

5.4 Clinical Relevance

Typical concentrations of total copper in serum of healthy individuals has been reported from 15.7 to 23.6 μM,[4, 225] with free copper ions constituting a small fraction of this total. In Wilson's disease and Autoimmune Hepatitis, free copper ion concentrations can rise to levels that are several times higher than those found in healthy individuals, often exceeding 2 μM.[4, 226] The Cu(II) ranges of 0 to 8 μM in HS detected in Paper III using MLP highlight similar concentration ranges observed in relation to such conditions.[4, 225, 226]

5.5 Network Architectures Beyond MLP

Beyond the MLP utilized in this work, other studies on architectures like Recurrent Neural Networks (RNNs) and Long Short-Term Memory (LSTM) networks have analyzed time-series data to identify trends, sensor degradation and contamination.[227, 228,229] By

continuously monitoring biosensor performance and adjusting parameters, machine learning ensures the sensor's accuracy and reliability over time.[230] The scalability of neural networks allows them to handle increasingly complex tasks and larger datasets, making them highly suitable for further applications to expand this work.

Chapter 6

6.0 Limitations and Future Outlook

The presented work contributes to biosensor development that enables detection of Cu(II) ions which has potential for clinical and environmental sample measurements.

While the developed ATCUN-based biosensor demonstrates significant promise, several limitations remain to be addressed in future work. The long-term stability of functionalized nanopore membranes and ATCUN-fluorophore conjugates is not comprehensively evaluated under varied environmental conditions, potentially limiting their shelf life and practical application in real-world settings such as clinical diagnostics or environmental monitoring. This might be achieved by modification of the ATCUN motif.

Though initial steps of using machine learning for the prediction of the Cu(II) concentration in fluids have been undertaken in this thesis, further refinement of such algorithms is needed to improve the data analysis. This would enhance the biosensor's ability to provide reliable results, even in complex biological matrices. The success of machine learning techniques in handling multiparameter and non-linear problems in biosensors has been demonstrated in several studies.[231-233]

Moreover, microfluidic system can be further optimized for enhanced resistance to biofouling when used with complex biological matrices. Miniaturization of the sensing platform through application-specific integrated circuits (ASICs) addresses portability limitations, while encapsulation technologies and stabilizing additives could extend operational lifetimes.

Further, incorporating the biosensor into wearable devices could provide continuous monitoring of copper levels in real time. This would be particularly beneficial for patients with conditions like

Wilson's disease, where copper levels need to be closely monitored. Recent advancements in wearable sensor platforms for real-time monitoring of metabolic disorders showcase the potential for such integration.[234,235] Additionally, a handheld sensing system based on infrared reflectivity measurement of the cornea has been proposed for non-invasive Wilson's disease progression monitoring.[236]

While the current focus is on copper ion detection, the platform's adaptability could allow for the detection of other biologically relevant metal ions. Recent research has demonstrated the potential for detecting various heavy metals in food and contaminated water using nanotechnological techniques.[234]

6.1 Commercialization and Clinical Trials

Transitioning biosensor technologies from laboratory research to clinical implementation necessitates rigorous evaluation through phased clinical trials alongside the integration of multimodal validation frameworks. Implementing orthogonal validation strategies—using independent methodological approaches to cross-verify critical biosensor performance parameters— enhances reliability for longitudinal monitoring applications where consistent analyte detection across fluctuating physiological conditions is paramount. Addressing these limitations through focused engineering efforts would significantly advance the transition from laboratory prototype to practical clinical tool. This approach has been demonstrated by validating insulin-peptide binding electrochemical assays with molecular dynamics simulations and thermodynamic profiling to identify context-dependent limitations of literature-reported biosensor.[237] Similarly, osteogenic differentiation biomarkers have been validated using SPR biosensors alongside RNA sequencing data, with machine learning models resolving technical variations between platforms.[238, 239] These approaches ensure robustness against methodological biases—a critical

requirement for biosensors deployed in chronic disease management where longitudinal data integrity directly impacts clinical decision-making.

Successful trials could lead to the commercialization of the biosensor, making it widely available for healthcare providers and patients. The biosimilar development and approval process, as regulated by both the US FDA and the European Medicines Agency, serves as a well-established model for efficiently bringing new biological products to market by demonstrating comparability to reference products through a rigorous, science-based evaluation.[240]

The future of this biosensor platform holds potential applications that could advance the way copper-related disorders are diagnosed and managed. The rapid evolution of biotechnology-derived medicinal products demonstrates the potential for innovative biosensor platforms to make significant impacts in healthcare.[240, 241] By continuing to innovate and expand its capabilities, this technology could play a crucial role in advancing personalized healthcare solutions.

References

1. Kim, B.-E.; Nevitt, T.; Thiele, D. J., Mechanisms for copper acquisition, distribution and regulation. *Nature Chemical Biology* **2008,** *4* (3), 176-185.

2. Li, Y.; Liang, J.; Chen, Y.; Wang, Y., The mechanism of copper homeostasis and its role in disease. **2023,** *1* (2), 109-120.

3. Falcone, E.; Vileno, B.; Hoang, M.; Raibaut, L.; Faller, P., A luminescent ATCUN peptide variant with enhanced properties for copper(II) sensing in biological media. *Journal of Inorganic Biochemistry* **2021,** *221*, 111478.

4. Gromadzka, G.; Grycan, M.; Przybyłkowski, A. M., Monitoring of Copper in Wilson Disease. **2023,** *13* (11), 1830.

5. Mandal, P. K.; Maroon, J. C.; Garg, A.; Arora, N. K.; Bansal, R.; Kaushik, A.; Samkaria, A.; Kumaran, G.; Arora, Y., Blood Biomarkers in Alzheimer's Disease. *ACS Chemical Neuroscience* **2023,** *14* (22), 3975-3978.

6. Fierke, C. A. In *Metal Ion Biosensor for Wastewater Discharge*, 2003.

7. Sheta, S. M.; El-Sheikh, S. M.; Abd-Elzaher, M. M., Simple synthesis of novel copper metal-organic framework nanoparticles: biosensing and biological applications. *Dalton Trans* **2018,** *47* (14), 4847-4855.

8. Chen, C.; Xu, H.; Zhan, Q.; Zhang, Y.; Wang, B.; Chen, C.; Tang, H.; Xie, Q., Preparation of novel HKUST-1-glucose oxidase composites and their application in biosensing. *Mikrochim Acta* **2022,** *190* (1), 10.

9. Shiu, W. T.; Chang, L. Y.; Jiang, Y.; Shakouri, M.; Wu, Y. H.; Lin, B. H.; Liu, L., Synthesis and characterization of a near-infrared persistent luminescent Cr-doped zinc gallate-calcium phosphate composite. *Phys Chem Chem Phys* **2022,** *24* (35), 21131-21140.

10. Wu, S.; Li, Y.; Ding, W.; Xu, L.; Ma, Y.; Zhang, L., Recent Advances of Persistent Luminescence Nanoparticles in Bioapplications. *Nanomicro Lett* **2020,** *12* (1), 70.

11. Filippidou, M. K.; Chatzandroulis, S., Microfluidic Devices for Heavy Metal Ions Detection: A Review. *Micromachines (Basel)* **2023,** *14* (8).

12. Jarczewska, M.; Szymczyk, A.; Zajda, J.; Olszewski, M.; Ziółkowski, R.; Malinowska, E., Recent Achievements in Electrochemical and Optical Nucleic Acids Based Detection of Metal Ions. *Molecules* **2022,** *27* (21).

13. Ghosh, S. Biosensors Market Outlook (2023 to 2033). https://www.futuremarketinsights.com/reports/biosensors-market#thankyou (accessed 09/13/2024).

14. Research, F. M. Biosensors for Point-of-Care Diagnostics Market. https://www.fairfieldmarketresearch.com/report/biosensors-for-point-of-care-diagnostics-market.

15. Mehrotra, P., Biosensors and their applications - A review. *Journal of oral biology and craniofacial research* **2016,** *6* (2), 153-9.

16. Valente, B.; Pinto, H.; Pereira, T. S.; Campos, R., Exploring Biosensors' Scientific Production and Research Patterns: A Bibliometric Analysis. **2024,** *24* (10), 3082.

17. Research, P. *Biosensors Market Size, Share, and Trends 2024 to 2034*; 1674; 2024.

18. Global, D. *Biosensors Market Size, Share, Growth, Statistics Analysis Report*; Website, 08/28/2023

2023; p 156.

19. Research, P. M. *iosensors Market Share, Size, Trends, Industry Analysis Report, By Application (Medical, Food Toxicity, Bioreactor, Agriculture, Environment, and Consumer Electronics); By End-Use; By Region; Segment Forecast, 2024 - 2032*; PM1936; Polaris Market Research Website, 03/2024, 2024; p 115.

20. Smutok, O.; Katz, E., Biosensors: Electrochemical Devices-General Concepts and Performance. *Biosensors (Basel)* **2022,** *13* (1).

21. Ramesh, M.; Janani, R.; Deepa, C.; Rajeshkumar, L., Nanotechnology-Enabled Biosensors: A Review of Fundamentals, Design Principles, Materials, and Applications. *Biosensors (Basel)* **2022,** *13* (1).

22. A Review of Biosensors and Their Applications. *ASME Open Journal of Engineering* **2023,** *2*.

23. Pohanka, M. J. I. J. o. E. S., Aptamers in Electrochemical Biosensors. **2022**.

24. Jiang, J.-H.; Tang, H., Bioanalytical Chemistry, Biosensors. In *Encyclopedia of Analytical Chemistry*, pp 1-28.

25. Naresh, V.; Lee, N., A Review on Biosensors and Recent Development of Nanostructured Materials-Enabled Biosensors. *Sensors (Basel)* **2021,** *21* (4).

26. Morales, M. A.; Halpern, J. M., Guide to Selecting a Biorecognition Element for Biosensors. *Bioconjug Chem* **2018,** *29* (10), 3231-3239.

27. Fdez-Sanromán, A.; Bernárdez-Rodas, N.; Rosales, E.; Pazos, M.; González-Romero, E.; Sanromán, M. Á., Biosensor Technologies for Water Quality: Detection of Emerging Contaminants and Pathogens. **2025,** *15* (3), 189.

28. Huang, C. W.; Lin, C.; Nguyen, M. K.; Hussain, A.; Bui, X. T.; Ngo, H. H., A review of biosensor for environmental monitoring: principle, application, and corresponding achievement of sustainable development goals. *Bioengineered* **2023,** *14* (1), 58-80.

29. Gui, Q.; Lawson, T.; Shan, S.; Yan, L.; Liu, Y., The Application of Whole Cell-Based Biosensors for Use in Environmental Analysis and in Medical Diagnostics. *Sensors (Basel)* **2017,** *17* (7).

30. Cybulski, P.; Bravo, M.; Chen, J. J.-K.; Van Zundert, I.; Krzyzowska, S.; Taemaitree, F.; Uji-i, H.; Hofkens, J.; Rocha, S.; Fortuni, B., Nanoparticle accumulation and penetration in 3D tumor models: the effect of size, shape, and surface charge. **2025,** *12*.

31. Qi, H.; Zhang, Z.; Li, Z.; Nan, H.; Bi, K.; Chen, Y., Synergic Effects of the Nanopore Size and Surface Charge on the Ion Selectivity of Graphene Membranes. *The Journal of Physical Chemistry C* **2021,** *125* (1), 507-514.

32. Venturoli, D.; Rippe, B., Ficoll and dextran vs. globular proteins as probes for testing glomerular permselectivity: effects of molecular size, shape, charge, and deformability. **2005,** *288* (4), F605-F613.

33. Agarwal, R.; and Roy, K., Intracellular Delivery of Polymeric Nanocarriers: a Matter of size, shape, charge, Elasticity and Surface Composition. *Therapeutic Delivery* **2013,** *4* (6), 705-723.

34. Yao, Y.; Wen, C.; Pham, N. H.; Zhang, S.-L., On Induced Surface Charge in Solid-State Nanopores. *Langmuir* **2020,** *36* (30), 8874-8882.

35. Brown, M. A.; Bossa, G. V.; May, S., Emergence of a Stern Layer from the Incorporation of Hydration Interactions into the Gouy–Chapman Model of the Electrical Double Layer. *Langmuir* **2015,** *31* (42), 11477-11483.

36. Zhang, Y.; Chen, X.; Wang, C.; Roozbahani, G. M.; Chang, H. C.; Guan, X., Chemically functionalized conical PET nanopore for protein detection at the single-molecule level. *Biosens Bioelectron* **2020,** *165*, 112289.

37. Lastra, L. S.; Sharma, V.; Farajpour, N.; Nguyen, M.; Freedman, K. J., Nanodiagnostics: A review of the medical capabilities of nanopores. *Nanomedicine* **2021,** *37*, 102425.

38. Zhao, M.; Zhang, Y.; Chen, L.; Yan, X.; Xu, T.; Fu, M.; Han, Y.; Zhang, Y.; Zhang, B.; Cao, J.; Lin, J.; Shen, D.; Li, S.; Zhu, C.; Zhao, W., Nanopore sequencing of

infectious fluid is a promising supplement for gold-standard culture in real-world clinical scenario. **2024,** *Volume 14 - 2024*.

39. Garcia-Calvo, E.; García-García, A.; Rodríguez, S.; Martín, R.; García, T., Unraveling the Properties of Phage Display Fab Libraries and Their Use in the Selection of Gliadin-Specific Probes by Applying High-Throughput Nanopore Sequencing. **2024,** *16* (5), 686.

40. Sen, A.; Shim, J.; Bala, A.; Park, H.; Kim, S. J. A. F. M., Boosting Sensitivity and Reliability in Field-Effect Transistor-Based Biosensors with Nanoporous MoS2 Encapsulated by Non-Planar Al2O3. **2023,** *33*.

41. Hintzen, J. C. J.; Devrani, S.; Carrod, A. J.; Bayik, M. B.; Tietze, D.; Tietze, A. A., Fluorescence Labeling of Peptides: Finding the Optimal Protocol for Coupling Various Dyes to ATCUN-like Structures. *ACS Organic & Inorganic Au* **2024**.

42. Liu, G.; Xia, N.; Tian, L.; Sun, Z.; Liu, L., Progress in the Development of Biosensors Based on Peptide–Copper Coordination Interaction. **2022,** *12* (10), 809.

43. Falcone, E.; Gonzalez, P.; Lorusso, L.; Seneque, O.; Faller, P.; Raibaut, L., A terbium(iii) luminescent ATCUN-based peptide sensor for selective and reversible detection of copper(ii) in biological media. *Chemical communications* **2020,** *56* (35), 4797-4800.

44. Muller, L. K.; Duznovic, I.; Tietze, D.; Weber, W.; Ali, M.; Stein, V.; Ensinger, W.; Tietze, A. A., Ultrasensitive and Selective Copper(II) Detection: Introducing a Bioinspired and Robust Sensor. *Chemistry* **2020,** *26* (39), 8511-8517.

45. Disorders of Copper Homeostasis. In *National Research Council (US) Committee on Copper in Drinking Water.* , Washington (DC): National Academies Press (US)

2000; Vol. 4, Disorders of Copper Homeostasis.

46. Kirsipuu, T.; Zadorožnaja, A.; Smirnova, J.; Friedemann, M.; Plitz, T.; Tõugu, V.; Palumaa, P., Copper(II)-binding equilibria in human blood. *Scientific Reports* **2020,** *10* (1), 5686.

47. Aronoff-Spencer, E.; Burns, C. S.; Avdievich, N. I.; Gerfen, G. J.; Peisach, J.; Antholine, W. E.; Ball, H. L.; Cohen, F. E.; Prusiner, S. B.; Millhauser, G. L., Identification of the Cu2+ Binding Sites in the N-Terminal Domain of the Prion Protein by EPR and CD Spectroscopy. *Biochemistry* **2000,** *39* (45), 13760-13771.

48. Pickart, L.; Margolina, A., Regenerative and Protective Actions of the GHK-Cu Peptide in the Light of the New Gene Data. **2018,** *19* (7), 1987.

49. Kotuniak, R.; Bal, W., Reactive Cu2+-peptide intermediates revealed by kinetic studies gain relevance by matching time windows in copper metallomics. *Metallomics* **2023,** *15* (2).

50. del Castillo-Velilla, I.; Sousaraei, A.; Romero-Muñiz, I.; Castillo-Blas, C.; S. J. Méndez, A.; Oropeza, F. E.; de la Peña O'Shea, V. A.; Cabanillas-González, J.; Mavrandonakis, A.; Platero-Prats, A. E., Synergistic binding sites in a metal-organic framework for the optical sensing of nitrogen dioxide. *Nature Communications* **2023,** *14* (1), 2506.

51. Evans, A.; Cummings, M.; Decarolis, D.; Gianolio, D.; Shahid, S.; Law, G.; Attfield, M.; Law, D.; Petit, C., Optimisation of Cu+ impregnation of MOF-74 to improve CO/N2 and CO/CO2 separations. *RSC Advances* **2020,** *10* (9), 5152-5162.

52. Zhang, W.; Tian, X.; Li, X., Fabrication of Nanocatalytic Medicine from Self-Assembling Peptides Containing an ATCUN-Like Copper-Binding Motif for Anticancer Therapy. *Chembiochem* **2024,** *25* (15), e202400216.

53. Duznovic, I.; Grawe, A.; Weber, W.; Muller, L. K.; Ali, M.; Ensinger, W.; Tietze, A.; Stein, V., Ultrasensitive and Selective Protein Recognition with Nanobody-Functionalized Synthetic Nanopores. *Small* **2021,** *17* (33), e2101066.

54. Zhang, H.; Zhao, T.; Huang, P.; Wang, Q.; Tang, H.; Chu, X.; Jiang, J., Spatiotemporally Resolved Protein Detection in Live Cells Using Nanopore Biosensors. *ACS Nano* **2022,** *16* (4), 5752-5763.

55. Mayer, M.; Semetey, V.; Gitlin, I.; Yang, J.; Whitesides, G. M., Using Ion Channel-Forming Peptides to Quantify Protein−Ligand Interactions. *J Am Chem Soc* **2008,** *130* (4), 1453-1465.

56. Yee, A. A.; Marat, K.; O'neil, J. D. J., The Interactions with Solvent, Heat Stability, and 13C-Labelling of Alamethicin, an Ion-Channel-Forming Peptide. **1997,** *243* (1-2), 283-291.

57. Engelberth, J.; Koch, T.; Schüler, G.; Bachmann, N.; Rechtenbach, J.; Boland, W., Ion channel-forming alamethicin is a potent elicitor of volatile biosynthesis and tendril coiling. Cross talk between jasmonate and salicylate signaling in lima bean. *Plant Physiol* **2001,** *125* (1), 369-77.

58. Su, Z.; Shodiev, M.; Leitch, J. J.; Abbasi, F.; Lipkowski, J., Role of Transmembrane Potential and Defects on the Permeabilization of Lipid Bilayers by Alamethicin, an Ion-Channel-Forming Peptide. *Langmuir* **2018,** *34* (21), 6249-6260.

59. Hsing, I. m. In *Smart Sensing Technologies for Point-of-Care Diagnostics*, 2012.

60. Liu, M.; Li, J.; Tan, C. S., Unlocking the Power of Nanopores: Recent Advances in Biosensing Applications and Analog Front-End. *Biosensors (Basel)* **2023,** *13* (6).

61. Lenhart, B.; Wei, X.; Zhang, Z.; Wang, X.; Wang, Q.; Liu, C., Nanopore Fabrication and Application as Biosensors in Neurodegenerative Diseases. *Critical reviews in biomedical engineering* **2020,** *48* (1), 29-62.

62. Ma, T.; Janot, J.-M.; Balme, S., Track-Etched Nanopore/Membrane: From Fundamental to Applications. **2020,** *4* (9), 2000366.

63. Kececi, K., A Comparable Study of Single Stranded DNA Sensing Using Track-Etched Nanopore Sensors. **2023,** *8* (37), e202302856.

64. Duznovic, I. Ion-conducting Nanopores in Polymer Membranes for (Bio)Molecular Sensory Applications. Ph.D. Thesis, Technische Universität Darmstadt, Darmstadt: University and State Library Darmstadt, 2021.

65. Zdorovets, M. V.; Korolkov, I. V.; Yeszhanov, A. B.; Gorin, Y. G., Functionalization of PET Track-Etched Membranes by UV-Induced Graft (co)Polymerization for Detection of Heavy Metal Ions in Water. *Polymers (Basel)* **2019,** *11* (11).

66. Nehra, A.; Chen, W.; Dimitrov, D. S.; Puri, A.; Singh, K. P., Graphene Oxide-Polycarbonate Track-Etched Nanosieve Platform for Sensitive Detection of Human Immunodeficiency Virus Envelope Glycoprotein. *ACS Applied Materials & Interfaces* **2017,** *9* (38), 32621-32634.

67. Dang, Q. M.; Wemple, A. H.; Leopold, M. C., Nanomaterial-Doped Xerogels for Biosensing Measurements of Xanthine in Clinical and Industrial Applications. **2023,** *9* (6), 437.

68. El Housseini, W.; Baiarashov, E.; Gerulskis, R.; Milam, A.; Minteer, S. D., Harnessing Redox Polymer Dynamics for Enhanced Glucose–Oxygen Coupling in Dual Biosensing and Therapeutic Applications. *ACS Sensors* **2024,** *9* (6), 3357-3366.

69. Yeh, S.-L.; Deval, P.; Wu, J.-G.; Luo, S.-C.; Tsai, W.-B., One-step electrochemical deposition of antifouling polymers with pyrogallol for biosensing applications. *Journal of Materials Chemistry B* **2022,** *10* (14), 2504-2511.

70. Chandra, A.; Datta, A., A Peptide-Based Fluorescent Sensor for Anionic Phospholipids. *ACS Omega* **2022,** *7* (12), 10347-10354.

71. Bohl, C.; Pomorski, A.; Seemann, S.; Knospe, A.-M.; Zheng, C.; Krężel, A.; Rolfs, A.; Lukas, J., Fluorescent probes for selective protein labeling in lysosomes: a case of α-galactosidase A. **2017,** *31* (12), 5258-5267.

72. Xiao, L.; Wei, P.; Yang, X.; Wang, P., A novel dual-signals peptide-based probe for highly selective detection of Cu(II) and glyphosate and its applications in smartphone-assisted test strips sensing system. *Microchemical Journal* **2023,** *193*, 109084.

73. Qian, B.; De Silva, S.; Reichman, S. M.; Bao, L.; Trinchi, A.; Lan, M.; Wei, G.; Váradi, L.; Cole, I., Development of SiO2-coumarin fluorescent nanohybrid and its application for Cu(II) sensing in aqueous extracts of roadside soil. *Journal of Nanoparticle Research* **2022,** *24* (6), 114.

74. Shalev, D. E., Studying Peptide-Metal Ion Complex Structures by Solution-State NMR. *Int J Mol Sci* **2022,** *23* (24).

75. Maiti, B. K.; Almeida, R. M.; Maia, L. B.; Moura, I.; Moura, J. J. G., Insights into the Molybdenum/Copper Heterometallic Cluster Assembly in the Orange Protein: Probing Intermolecular Interactions with an Artificial Metal-Binding ATCUN Tag. *Inorganic chemistry* **2017,** *56* (15), 8900-8911.

76. Frączyk, T., Phosphorylation Impacts Cu(II) Binding by ATCUN Motifs. *Inorganic chemistry* **2021,** *60* (12), 8447-8450.

77. Pushie, M. J.; Stefaniak, E.; Sendzik, M. R.; Sokaras, D.; Kroll, T.; Haas, K. L., Using N-Terminal Coordination of Cu(II) and Ni(II) to Isolate the Coordination Environment of Cu(I) and Cu(II) Bound to His13 and His14 in Amyloid-β(4-16). *Inorganic chemistry* **2019,** *58* (22), 15138-15154.

78. Schlotter, T.; Kloter, T.; Hengsteler, J.; Yang, K.; Zhan, L.; Ragavan, S.; Hu, H.; Zhang, X.; Duru, J.; Vörös, J.; Zambelli, T.; Nakatsuka, N., Aptamer-Functionalized Interface Nanopores Enable Amino Acid-Specific Peptide Detection. *ACS Nano* **2024,** *18* (8), 6286-6297.

79. Kaya, D.; Cayón, V. M.; Trautmann, C.; Toimil Molares, M. E., Biosensing with Tailored Track-Etched Nanochannels. *ECS Meeting Abstracts* **2023,** *MA2023-02* (57), 2785.

80. Shanbhag, M. M.; Manasa, G.; Mascarenhas, R. J.; Mondal, K.; Shetti, N. P., Fundamentals of bio-electrochemical sensing. *Chemical Engineering Journal Advances* **2023,** *16*, 100516.

81. Girigoswami, K.; Akhtar, N. J. i. j. o. n. d., Nanobiosensors and fluorescence based biosensors: An overview. **2019,** *10*, 1-17.

82. Damborský, P.; Švitel, J.; Katrlík, J., Optical biosensors. *Essays in biochemistry* **2016,** *60* (1), 91-100.

83. Lee, M.; Shin, S.; Kim, S.; Park, N., Recent Advances in Biological Applications of Aptamer-Based Fluorescent Biosensors. *Molecules* **2023,** *28* (21).

84. Xiong, Y.; Shepherd, S.; Tibbs, J.; Bacon, A.; Liu, W.; Akin, L. D.; Ayupova, T.; Bhaskar, S.; Cunningham, B. T., Photonic Crystal Enhanced Fluorescence: A Review on Design Strategies and Applications. *Micromachines (Basel)* **2023,** *14* (3).

85. Rupcich, N.; Chiuman, W.; Nutiu, R.; Mei, S.; Flora, K. K.; Li, Y.; Brennan, J. D., Quenching of fluorophore-labeled DNA oligonucleotides by divalent metal ions: implications for selection, design, and applications of signaling aptamers and signaling deoxyribozymes. *J Am Chem Soc* **2006,** *128* (3), 780-90.

86. Satishkumar, B. C.; Brown, L. O.; Gao, Y.; Wang, C. C.; Wang, H. L.; Doorn, S. K., Reversible fluorescence quenching in carbon nanotubes for biomolecular sensing. *Nat Nanotechnol* **2007,** *2* (9), 560-4.

87. Wang, M.; Zhao, Z.; Gong, W.; Zhang, M.; Lu, N., Modulating the Biomimetic and Fluorescence Quenching Activities of Metal-Organic Framework/Platinum Nanoparticle Composites and Their Applications in Molecular Biosensing. *ACS Appl Mater Interfaces* **2022,** *14* (18), 21677-21686.

88. Battisti, A.; Samal, S. K.; Puppi, D., Biosensing Systems Based on Graphene Oxide Fluorescence Quenching Effect. *Micromachines (Basel)* **2023,** *14* (8).

89. Lee, Y. J.; Kim, Y.; Kim, H.; Choi, J.; Noh, G. H.; Lee, K.-S.; Lee, J.; Choi, C. H.; Kim, S. H.; Seo, J., Unlocking Cu(I)-Mediated Catalytic Pathways for Efficient ROS Generation by Incorporating an Oxazole-Based Histidine Surrogate into Cu(II)–ATCUN Complexes. *Inorganic chemistry* **2023,** *62* (26), 10279-10290.

90. Kreuzer, M. P.; McCarthy, R.; Pravda, M.; Guilbault, G. G., Development of Electrochemical Immunosensor for Progesterone Analysis in Milk. *Analytical Letters* **2004,** *37* (5), 943-956.

91. Melikishvili, S.; Hianik, T.; Thompson, M., Detection of Sub-Nanomolar Concentration of Trypsin by Thicken-Shear Mode (TSM) Acoustic Wave Biosensor. **2020,** *60* (1), 6.

92. Masdor, N. A., Detection Limit of the Four-Parameter Logistic Model for the Quantitative Detection of Serum Squamous Cell Carcinoma Antigenin Cervical Cancer Based on Surface Plasmon Resonance Biosensor. *Journal of Environmental Microbiology and Toxicology* **2021,** *9* (2), 30-32.

93. Rouaud, F.; Tessaro, F.; Aimaretti, L.; Scapozza, L.; Citi, S., Cooperative binding of the tandem WW domains of PLEKHA7 to PDZD11 promotes conformation-dependent interaction with tetraspanin 33. *J Biol Chem* **2020,** *295* (28), 9299-9312.

94. Uba, G.; Yakasai, H. M.; Abubakar, A., Limits of Detection Determination of Aflatoxin B1 using the Optical Waveguide Lightmode Spectroscopy via the Four-Parameter Logistic Model. *Bioremediation Science and Technology Research* **2022,** *10* (2), 40-44.

95. Fairbairn, C. E.; Kang, D., Temporal Dynamics of Transdermal Alcohol Concentration Measured via New-Generation Wrist-Worn Biosensor. **2019,** *43* (10), 2060-2069.

96. Hahn, D. H. U. K. S. M. S. J. J., Data-Driven Modeling in Biomedical Applications: The Search for Biomarkers in Autism Spectrum Disorder. Institute, R. P., Ed. 2016; p 6.

97. Jagannatha, S.; Sargsyan, D.; Manyakov, N. V.; Skalkin, A.; Bangerter, A.; Ness, S.; Lewin, D.; Johnson, K.; Durham, K.; Pandina, G., A Practical Application of Data Mining Methods to Build Predictive Models for Autism Spectrum Disorder Based on Biosensor Data From Janssen Autism Knowledge Engine (JAKE®). *Statistics in Biopharmaceutical Research* **2019,** *11* (2), 111-117.

98. Zhang, J.; Srivatsa, P.; Ahmadzai, F. H.; Liu, Y.; Song, X.; Karpatne, A.; Kong, Z.; Johnson, B. N., Reduction of Biosensor False Responses and Time Delay Using Dynamic Response and Theory-Guided Machine Learning. *ACS Sens* **2023,** *8* (11), 4079-4090.

99. Cho, Y.; Kwak, I. H.; Kim, D.; Na, J.; Sung, H.; Lee, J.; Kim, Y. E.; Ma, H.-I. J. A., Statistical Analysis by Semiparametric Additive Regression and LSTM-FCN Based Hierarchical Classification for Computer Vision Quantification of Parkinsonian Bradykinesia. **2024,** *abs/2404.00670*.

100. Schackart, K. E., 3rd; Yoon, J. Y., Machine Learning Enhances the Performance of Bioreceptor-Free Biosensors. *Sensors (Basel)* **2021,** *21* (16).

101. Tahaseen, M.; Moparthi, N. R. J. t. I. C. o. E., Communication; Technology, A., An Assessment of the Machine Learning Algorithms Used in Agriculture. **2021**, 1579-1584.

102. Bhalla, N. J. A. S. R., Measurement of Human Urine Specific Gravity Using Nanoplasmonics: A Paradigm Shift from Scales to Biosensors. **2024,** *3*.

103. Rathi, S. R.; Kshirsagar, P. S.; Mandhare, A.; Jagadale, P.; Patil, K.; Nakate, S. J. r. I. C. o. I. M. f. I. A., An Analysis of the Performance of Machine Learning Algorithms for Prediction of Lung Cancer. **2023**, 967-972.

104. Ogundunmade, T. P.; Adepoju, A. A. J. I. J. o. C. E., Modelling Credit Card Fraud Data using Machine Learning Algorithms. **2024**.

105. Ebrahim, O. A.; Derbew, G., Application of supervised machine learning algorithms for classification and prediction of type-2 diabetes disease status in Afar regional state, Northeastern Ethiopia 2021. *Sci Rep* **2023,** *13* (1), 7779.

106. Xu, R.; Chen, Y.; Yao, Z.; Wu, W.; Cui, J.; Wang, R.; Diao, Y.; Jin, C.; Hong, Z.; Li, X., Application of machine learning algorithms to identify people with low bone density. *Front Public Health* **2024,** *12*, 1347219.

107. Kruse, R.; Borgelt, C.; Braune, C.; Mostaghim, S.; Steinbrecher, M., Introduction to Neural Networks. In *Computational Intelligence: A Methodological Introduction*, Kruse, R.; Borgelt, C.; Braune, C.; Mostaghim, S.; Steinbrecher, M., Eds. Springer London: London, 2016; pp 9-13.

108. Liang, Z. J. H. i. B., Economics; Management, Predict Customer Churn based on Machine Learning Algorithms. **2023**.

109. Mota, M. J. S.; Vieira, A. C. A.; Lima, L. S.; Sátiro, J. V. M.; Menezes Neto, C. M. d.; Paixão, P. L. P.; Lopes, G. P. G.; Setton, L. R. d. A.; Andrade, C. E. d.; Cabral, R. H. J. J. A. o. H., Sex determination based on craniometric parameters: a comparative approach between linear and non-linear machine learning algorithms. **2024**.

110. Leng, X.; Shi, R.; Wu, Y.; Zhu, S.; Cai, X.; Lu, X.; Liu, R., Deep learning for detection of age-related macular degeneration: A systematic review and meta-analysis of diagnostic test accuracy studies. *PLoS One* **2023,** *18* (4), e0284060.

111. Chen, Z.; Zhang, L.; Sun, J.; Meng, R.; Yin, S.; Zhao, Q., DCAMCP: A deep learning model based on capsule network and attention mechanism for molecular carcinogenicity prediction. *Journal of cellular and molecular medicine* **2023,** *27* (20), 3117-3126.

112. Xu, Y.; Kuang, L.; Zhu, T.; Zeng, J.; Georgiou, P. J. I. I. S. o. C.; Systems, Drift Prediction and Chemical Reaction Identification for ISFETs using Deep Learning. **2023**, 1-5.

113. Kaziz, S.; Jemmali, A.; Echouchene, F., Optimization of annular microfluidic biosensor enhanced by active and passive effects using Taguchi's method coupled with multi-layer perceptron neural networks (MLP-NN) models. *Microfluidics and Nanofluidics* **2023,** *27* (9), 60.

114. Huang, Y.; Darr, C. M.; Gangopadhyay, K.; Gangopadhyay, S.; Bok, S.; Chakraborty, S., Applications of machine learning tools for ultra-sensitive detection of lipoarabinomannan with plasmonic grating biosensors in clinical samples of tuberculosis. *PLoS One* **2022,** *17* (10), e0275658.

115. Macchia, E.; Kovács-Vajna, Z. M.; Loconsole, D.; Sarcina, L.; Redolfi, M.; Chironna, M.; Torricelli, F.; Torsi, L., A handheld intelligent single-molecule binary bioelectronic system for fast and reliable immunometric point-of-care testing. **2022,** *8* (27), eabo0881.

116. Abd Al-Rahman, S. Q.; Hasan, E. H.; Sagheer, A. M. J. I. I. J. o. A. I., Design and implementation of the web (extract, transform, load) process in data warehouse application. **2023**.

117. Dingre, S. S. J. J. o. A. I.; amp; Computing, C., Internal Controls in the ETL Process. **2023**.

118. Almeida, J. R.; Pazos, A.; Oliveira, J. L. In *Harmonising Alzheimer's Disease Cohorts using a Common ETL Tool*, 2022.

119. Lam, S. S. W.; Fang, A. H. S.; Koh, M. S.; Shantakumar, S.; Yeo, S. H.; Matchar, D. B.; Ong, M. E. H.; Poon, K. M. T.; Huang, L.; Harikrishan, S.; Milea, D.; Burke, D.; Webb, D.; Ragavendran, N.; Tan, N. C.; Loo, C. M., Development of a real-world database for asthma and COPD: The SingHealth-Duke-NUS-GSK COPD and Asthma Real-World Evidence (SDG-CARE) collaboration. *BMC medical informatics and decision making* **2023,** *23* (1), 4.

120. Lemordant, P.; Bouzille, G.; Mathieu, R.; Thenault, R.; Gibaud, B.; Garde, C.; Campillo-Gimenez, B.; Goudet, D.; Delarche, S.; Roland, Y.; Cuggia, M., How to Optimize Connection Between PACS and Clinical Data Warehouse: A Web Service Approach Based on Full Metadata Integration. *Studies in health technology and informatics* **2022,** *290*, 27-31.

121. Ta'a, A.; Ishak, N.; Elias, E. M.; Mahidin, N. J. J. o. I. S.; Management, T., AN IMPACT ANALYSIS OF EXTRACT TRANSFORM LOAD PROCESS FOR MAINTAINING THE SYSTEM OF DATA WAREHOUSE. **2022**.

122. Bryce, D.; Goldman, R. P.; DeHaven, M.; Beal, J.; Bartley, B.; Nguyen, T. T.; Walczak, N.; Weston, M.; Zheng, G.; Nowak, J.; Lee, P.; Stubbs, J.; Gaffney, N.; Vaughn, M. W.; Myers, C. J.; Moseley, R. C.; Haase, S.; Deckard, A.; Cummins, B.; Leiby, N., Round Trip: An Automated Pipeline for Experimental Design, Execution, and Analysis. *ACS Synthetic Biology* **2022,** *11* (2), 608-622.

123. Zborowski, T. In *Automation of xMAP ® Technology-Based Multiplex Assays*, 2016.

124. Marzuki, K.; Kholid, M. I.; Zazuli, L.; Mardedi, A.; Info, A. J. I. J. o. E.; Systems, C., Automation of Open VSwitch-Based Virtual Network Configuration Using Ansible on Proxmox Virtual Environment. **2023**.

125. Rezvani, K.; Smith, A.; Javed, J.; Keller, W. R.; Stewart, K. D.; Kim, L.; Newell, K. J., Demonstration of continuous gradient elution functionality with automated liquid handling systems for high-throughput purification process development. *Journal of Chromatography A* **2023,** *1687*, 463658.

126. Raju, C. M.; Elpa, D. P.; Urban, P. L., Automation and Computerization of (Bio)sensing Systems. *ACS Sensors* **2024,** *9* (3), 1033-1048.

127. Rigoulot, S. B.; Park, J.; Fabish, J.; Seaberry, E. M.; Parrish, A.; Meier, K. A.; Whinna, R.; Dong, S., Enabling High-throughput Transgene Expression Studies Using Automated Liquid Handling for Etiolated Maize Leaf Protoplasts. *J Vis Exp* **2024,** (204).

128. Jenne, A.; von der Ecken, S.; Moxley-Paquette, V.; Soong, R.; Swyer, I.; Bastawrous, M.; Busse, F.; Bermel, W.; Schmidig, D.; Kuehn, T.; Kuemmerle, R.; Al Adwan-Stojilkovic, D.; Graf, S.; Frei, T.; Monette, M.; Wheeler, A. R.; Simpson, A. J., Integrated Digital Microfluidics NMR Spectroscopy: A Key Step toward Automated In Vivo Metabolomics. *Analytical Chemistry* **2023,** *95* (14), 5858-5866.

129. Schmidt-Speicher, L. M.; Länge, K., Microfluidic integration for electrochemical biosensor applications. *Current Opinion in Electrochemistry* **2021,** *29*, 100755.

130. Kiani, M. J.; Dehghan, A.; Saadatbakhsh, M.; Jamali Asl, S.; Nouri, N. M.; Pishbin, E., Robotic digital microfluidics: a droplet-based total analysis system. *Lab on a Chip* **2023,** *23* (4), 748-760.

131. White, I., *Optofluidic biosensing for the study of disease at the molecular level*. SPIE: 2010; Vol. 7606.

132. Gerdan, Z.; Saylan, Y.; Denizli, A., Biosensing Platforms for Cardiac Biomarker Detection. *ACS Omega* **2024,** *9* (9), 9946-9960.

133. Lu, H.; Rakhymzhanov, A.; Buttner, U.; Alsulaiman, D., Making Healthcare Accessible: A Rapid Clean-Room-Free Fabrication Strategy for Microfluidics-Driven Biosensors Based on Coupling Stereolithography and Hot Embossing. *ACS Omega* **2024,** *9* (36), 38096-38106.

134. Dimov, N.; McDonnell, M. B.; Munro, I.; McCluskey, D. K.; Johnston, I. D.; Tan, C. K. L.; Coudron, L., *Electrowetting-based Digital Microfluidics Platform for Automated Enzyme-linked Immunosorbent Assay*. 1940-087X: 2020; Vol. 156 %J JoVE, p e60489.

135. Ott, O.; Tolppi, S.; Figueroa-Cruz, J.; Myagmar, K.; Unurbuyan, K.; Tripathi, A., Leveraging the fundamentals of heat transfer and fluid mechanics in microscale geometries for automated next-generation sequencing library preparation. *Sci Rep* **2024,** *14* (1), 12564.

136. Das, D.; Masetty, M.; Priye, A., Paper-Based Loop Mediated Isothermal Amplification (LAMP) Platforms: Integrating the Versatility of Paper Microfluidics with Accuracy of Nucleic Acid Amplification Tests. **2023,** *11* (3), 163.

137. Magro, L.; Escadafal, C.; Garneret, P.; Jacquelin, B.; Kwasiborski, A.; Manuguerra, J.-C.; Monti, F.; Sakuntabhai, A.; Vanhomwegen, J.; Lafaye, P.; Tabeling, P., Paper microfluidics for nucleic acid amplification testing (NAAT) of infectious diseases. *Lab on a Chip* **2017,** *17* (14), 2347-2371.

138. Fu, Y.; Finney, N. S., Small-molecule fluorescent probes and their design. *RSC Advances* **2018,** *8* (51), 29051-29061.

139. Beija, M.; Afonso, C. A. M.; Martinho, J. M. G., Synthesis and applications of Rhodamine derivatives as fluorescent probes. *Chemical Society Reviews* **2009,** *38* (8), 2410-2433.

140. Loudet, A.; Burgess, K., BODIPY Dyes and Their Derivatives: Syntheses and Spectroscopic Properties. *Chemical Reviews* **2007,** *107* (11), 4891-4932.

141. Wei, P.; Xiao, L.; Hou, P.; Wang, Q.; Wang, P., A novel Cu(II)-assisted peptide fluorescent probe for highly sensitive detection of glyphosate in real samples: real application in test strips and smartphone. *Analytical and Bioanalytical Chemistry* **2023,** *415* (24), 5985-5996.

142. Rai, R. K.; De Angelis, A.; Greenwood, A.; Opella, S. J.; Cotten, M. L., Metal-ion Binding to Host Defense Peptide Piscidin 3 Observed in Phospholipid Bilayers by Magic Angle Spinning Solid-state NMR. **2019,** *20* (2), 295-301.

143. Fu, R.; Rooney, M. T.; Zhang, R.; Cotten, M. L., Coordination of Redox Ions within a Membrane-Binding Peptide: A Tale of Aromatic Rings. *The Journal of Physical Chemistry Letters* **2021,** *12* (18), 4392-4399.

144. Zhou, J.; Chu, C.-Y. J. Q. N., ONE-POT SYNTHESIS OF A REVERSIBLE AND SENSITIVE FLUORESCENT PROBE FOR THE DETECTION OF MALACHITE GREEN. **2023**.

145. Xiao, S.; Sun, L.; Kang, M.; Dong, Z., A label-free aptasensor for clenbuterol detection based on fluorescence resonance energy transfer between graphene oxide and rhodamine B. *RSC Advances* **2022,** *12* (50), 32737-32743.

146. Deng, D.; Hao, Y.; Yang, P.; Xia, N.; Yu, W.; Liu, X.; Liu, L., Single-labeled peptide substrates for detection of protease activity based on the inherent fluorescence quenching ability of Cu2+. *Anal Methods-Uk* **2019,** *11* (9), 1248-1253.

147. Noormägi, A.; Golubeva, T.; Berntsson, E.; Wärmländer, S. K. T. S.; Tõugu, V.; Palumaa, P., Direct Competition of ATCUN Peptides with Human Serum Albumin for Copper(II) Ions Determined by LC-ICP MS. *ACS Omega* **2023,** *8* (37), 33912-33919.

148. Mueller, L. In *Chemical synthesis of switchable peptide-based nanopores: from ion channels to bio-inspired materials*, 2019.

149. Sahoo, A. K. In *Mixed Ligand Complex of Copper (II) Containing O-N Donor Ligands*, 2009.

150. Stokowa-Sołtys, K.; Szczerba, K.; Pacewicz, M.; Wieczorek, R.; Wezynfeld, N. E.; Bal, W., Interactions of neurokinin B with copper(ii) ions and their potential biological consequences. *Dalton Transactions* **2022,** *51* (37), 14267-14276.

151. Kotuniak, R.; Bal, W., Kinetics of Cu(ii) complexation by ATCUN/NTS and related peptides: a gold mine of novel ideas for copper biology. *Dalton Transactions* **2022,** *51* (1), 14-26.

152. Gasmi, G.; Singer, A.; Forman-Kay, J.; Sarkar, B., NMR structure of neuromedin C, a neurotransmitter with an amino terminal CuII-, NiII-binding (ATCUN) motif. *The journal of peptide research : official journal of the American Peptide Society* **1997,** *49* (6), 500-9.

153. Domergue, J.; Guinard, P.; Douillard, M.; Pécaut, J.; Hostachy, S.; Proux, O.; Lebrun, C.; Le Goff, A.; Maldivi, P.; Duboc, C.; Delangle, P., A Series of Ni Complexes Based on a Versatile ATCUN-Like Tripeptide Scaffold to Decipher Key Parameters for Superoxide Dismutase Activity. *Inorganic chemistry* **2023,** *62* (23), 8747-8760.

154. Munshi, M. U.; Berden, G.; Oomens, J., Facial vs. meridional coordination in gaseous Ni(ii)–hexacyclen complexes revealed with infrared ion spectroscopy. *Physical Chemistry Chemical Physics* **2022,** *24* (43), 26890-26897.

155. Jarockyte, G.; Karabanovas, V.; Rotomskis, R.; Mobasheri, A., Multiplexed Nanobiosensors: Current Trends in Early Diagnostics. *Sensors (Basel)* **2020,** *20* (23).

156. Ferrell, J. E., Jr., Q&A: Cooperativity. *Journal of biology* **2009,** *8* (6), 53.

157. Heinrich, J.; Bossak-Ahmad, K.; Riisom, M.; Haeri, H. H.; Steel, T. R.; Hergl, V.; Langhans, A.; Schattschneider, C.; Barrera, J.; Jamieson, S. M. F.; Stein, M.; Hinderberger, D.; Hartinger, C. G.; Bal, W.; Kulak, N., Incorporation of β-Alanine in Cu(II) ATCUN Peptide Complexes Increases ROS Levels, DNA Cleavage and Antiproliferative Activity. **2021,** *27* (72), 18093-18102.

158. Choi, S.; Juan, J. A. S.; Heffern, M. C.; Stevenson, M. J., Quantifying the Binding Interactions Between Cu(II) and Peptide Residues in the Presence and Absence of Chromophores. *JoVE* **2022,** (182), e63668.

159. Xie, M.; Chen, Z.; Zhao, F.; Lin, Y.; Zheng, S.; Han, S., Selection and Application of ssDNA Aptamers for Fluorescence Biosensing Detection of Malachite Green. **2022,** *11* (6), 801.

160. Lu, X.; Dong, X.; Zhang, K.; Han, X.; Fang, X.; Zhang, Y., A gold nanorods-based fluorescent biosensor for the detection of hepatitis B virus DNA based on fluorescence resonance energy transfer. *Analyst* **2013,** *138* (2), 642-650.

161. Liu, L.; Fang, Z.; Zheng, X.; Xi, D., Nanopore-Based Strategy for Sensing of Copper(II) Ion and Real-Time Monitoring of a Click Reaction. *ACS Sensors* **2019,** *4* (5), 1323-1328.

162. Devrani, S.; Tietze, D.; Tietze, A. A., Automated Microfluidic Platform for High-Throughput Biosensor Development. **2025,** *4* (3), 2400116.

163. Glatz, R. T.; Ates, H. C.; Mohsenin, H.; Weber, W.; Dincer, C., Designing electrochemical microfluidic multiplexed biosensors for on-site applications. *Anal Bioanal Chem* **2022,** *414* (22), 6531-6540.

164. Glatz, R. T.; Ates, H. C.; Mohsenin, H.; Weber, W.; Dincer, C., Designing electrochemical microfluidic multiplexed biosensors for on-site applications. *Analytical and Bioanalytical Chemistry* **2022,** *414* (22), 6531-6540.

165. Dushek, O.; Lellouch, A. C.; Vaux, D. J.; Shahrezaei, V., Biosensor architectures for high-fidelity reporting of cellular signaling. *Biophys J* **2014,** *107* (3), 773-782.

166. Vaneev, A. N.; Timoshenko, R. V.; Gorelkin, P. V.; Klyachko, N. L.; Erofeev, A. S., Recent Advances in Nanopore Technology for Copper Detection and Their Potential Applications. *Nanomaterials (Basel)* **2023,** *13* (9).

167. <Dissertation_Ivana_V3.pdf>.

168. Pardehkhorram, R.; Andrieu-Brunsen, A., Pushing the limits of nanopore transport performance by polymer functionalization. *Chemical communications* **2022,** *58* (34), 5188-5204.

169. Falcone, E.; Gonzalez, P.; Lorusso, L.; Sénèque, O.; Faller, P.; Raibaut, L., A terbium(iii) luminescent ATCUN-based peptide sensor for selective and reversible detection of copper(ii) in biological media. *Chemical communications* **2020,** *56* (35), 4797-4800.

170. Jankovic, S. J. I. J. o. B.; Healthcare, Tests for Comparison of Two Groups: Student's T-test, Mann-Whitney U-test and Chi-square Test. **2022**.

171. Peró-Cebollero, M.; Guàrdia-Olmos, J. J. P., The adequacy of different robust statistical tests in comparing two independent groups. **2013,** *34*, 407-424.

172. Boscardin, C. K.; Sewell, J. L.; Tolsgaard, M. G.; Pusic, M. V., How to Use and Report on p-values. *Perspectives on Medical Education* **2024**.

173. Nien Hsuan, C.; Jung Chuan, C.; Tai Ping, S.; Shen Kan, H., Measurement and comparison of potentiometric selectivity coefficients of urea biosensors based on ammonium ion-selective electrodes. *IEEE Sensors Journal* **2005,** *5* (6), 1362-1368.

174. Kim, H.; Jang, J. H.; Jung, I. Y.; Cho, J. H., A Novel Peptide as a Specific and Selective Probe for Klebsiella pneumoniae Detection. **2022,** *12* (3), 153.

175. Paul, S.; Nandi, S.; Das, M.; Bora, A.; Hossain, M. T.; Ghosh, S.; Giri, P. K., Two-dimensional bismuth oxyselenide quantum dots as nanosensors for selective metal ion detection over a wide dynamic range: sensing mechanism and selectivity. *Nanoscale* **2023,** *15* (30), 12612-12625.

176. Santos, A. O.; Abrantes-Coutinho, V. E.; Morais, S.; Oliveira, T., Agaricus bisporus Wild Mushroom Extract as Lectin Source for Engineering a Lactose Photoelectrochemical Biosensor. *Biosensors (Basel)* **2023,** *13* (2).

177. Dehdar, S.; Salimifard, K.; Mohammadi, R.; Marzban, M.; Saadatmand, S.; Fararouei, M.; Dianati-Nasab, M., Applications of different machine learning approaches in prediction of breast cancer diagnosis delay. **2023,** *13*.

178. Ljubobratović, D.; Vuković, M.; Brkić Bakarić, M.; Jemrić, T.; Matetić, M., Assessment of Various Machine Learning Models for Peach Maturity Prediction Using Non-Destructive Sensor Data. **2022,** *22* (15), 5791.

179. Vallée, R.; Vallée, J.-N.; Guillevin, C.; Lallouette, A.; Thomas, C.; Rittano, G.; Wager, M.; Guillevin, R.; Vallée, A., Machine learning decision tree models for multiclass classification of common malignant brain tumors using perfusion and spectroscopy MRI data. **2023,** *13*.

180. Gimati, Y. M. T. J. G. J. o. E.; Advances, T., Comparison estimating of classification error rate in decision tree: Data mining. **2021**.

181. Mohanapriya, M.; Lekha, J., Comparative study between decision tree and knn of data mining classification technique. *Journal of Physics: Conference Series* **2018,** *1142* (1), 012011.

182. Rowe, S. M.; Zhang, E.; Godden, S. M.; Vasquez, A. K.; Nydam, D. V., Comparison of a machine learning model with a conventional rule-based selective dry cow therapy algorithm for detection of intramammary infections. *Journal of Dairy Science* **2024**.

183. Iván-Baragaño, I.; Maneiro, R.; Losada, J. L.; Casal, C. A.; Ardá, A., Technical–tactical differences between female and male elite football: A data mining approach through neural network analysis, binary logistic regression, and decision tree techniques. *0* (0), 17543371241254602.

184. Jomtarak, R.; Kittichai, V.; Pengsakul, T.; Phatthamolrat, N.; Naing, K. M.; Tongloy, T.; Chuwongin, S.; Boonsang, S. J. b., Performance of deep convolutional neural network approaches and human level in detecting mosquito species. **2021**.

185. Yang, W.-J.; Wu, L.; Mei, Z.-M.; Xiang, Y., The Application of Artificial Neural Networks and Logistic Regression in the Evaluation of Risk for Dry Eye after Vitrectomy. **2020,** *2020* (1), 1024926.

186. Qu, S.; Zhou, M.; Jiao, S.; Zhang, Z.; Xue, K.; Long, J.; Zha, F.; Chen, Y.; Li, J.; Yang, Q.; Wang, Y., Optimizing acute stroke outcome prediction models: Comparison of generalized regression neural networks and logistic regressions. *PLOS ONE* **2022,** *17* (5), e0267747.

187. Issitt, R. W.; Cortina-Borja, M.; Bryant, W.; Bowyer, S.; Taylor, A. M.; Sebire, N., Classification Performance of Neural Networks Versus Logistic Regression Models: Evidence From Healthcare Practice. *Cureus* **2022,** *14* (2), e22443.

188. Becerra, V. M.; Garces, F. R.; Nasuto, S. J.; Holderbaum, W., An efficient parameterization of dynamic neural networks for nonlinear system identification. *IEEE Transactions on Neural Networks* **2005,** *16* (4), 983-988.

189. Chen, S.; Billings, S. A.; Grant, P. M., Non-linear system identification using neural networks. *International Journal of Control* **1990,** *51* (6), 1191-1214.

190. Therrien, R.; Doyle, S., *Role of training data variability on classifier performance and generalizability*. SPIE: 2018; Vol. 10581.

191. Zhang, S.; Liu, Y.; Sun, Y.; Shah, N. J. A., Graph-less Neural Networks: Teaching Old MLPs New Tricks via Distillation. **2021,** *abs/2110.08727*.

192. Mostafa, N.; Aly, W. H. F.; Alabed, S.; Al-Arnaout, Z., Intelligent Replica Selection in Edge and IoT Environments Using Artificial Neural Networks. **2022,** *11* (16), 2531.

193. Reddy, A. V.; Shah, K.; Paul, W.; Mocharla, R.; Hoffman, J.; Katyal, K. D.; Manocha, D.; Melo, C. M. d.; Chellappa, R. J. I. I. C. o. R.; Automation, Synthetic-to-Real Domain Adaptation for Action Recognition: A Dataset and Baseline Performances. **2023**, 11374-11381.

194. Buhot, A., Advances in Amplification Methods for Biosensors. *Biosensors (Basel)* **2023,** *13* (3).

195. Sharma, A.; Badea, M.; Tiwari, S.; Marty, J. L., Wearable Biosensors: An Alternative and Practical Approach in Healthcare and Disease Monitoring. **2021,** *26* (3), 748.

196. Buttkewitz, M. A.; Heuer, C.; Bahnemann, J., Sensor integration into microfluidic systems: trends and challenges. *Current Opinion in Biotechnology* **2023,** *83*, 102978.

197. Özkayar, G.; Lötters, J. C.; Tichem, M.; Ghatkesar, M. K., Toward a modular, integrated, miniaturized, and portable microfluidic flow control architecture for organs-on-chips applications. *Biomicrofluidics* **2022,** *16* (2).

198. Huang, X.; Pan, Y.; Zhang, G. L.; Li, B.; Guo, W.; Ho, T.-Y.; Schlichtmann, U. J. I. T. o. C.-A. D. o. I. C.; Systems, PathDriver+: Enhanced Path-Driven Architecture Design for Flow-Based Microfluidic Biochips. **2022,** *41*, 2185-2198.

199. Vijayakumar, M.; Rohita, D. S.; Rao, T. N.; Karthik, M., Electrode mass ratio impact on electrochemical capacitor performance. *Electrochimica Acta* **2019,** *298*, 347-359.

200. Zhang, J.; Jiang, J.; Li, H.; Zhao, X. S., A high-performance asymmetric supercapacitor fabricated with graphene-based electrodes. *Energy & Environmental Science* **2011,** *4* (10), 4009-4015.

201. Li, J.; Tang, J.; Yuan, J.; Zhang, K.; Sun, Y.; Zhang, H.; Qin, L.-C., Enlarging energy density of supercapacitors using unequal graphene electrodes and ionic liquid electrolyte. *Electrochimica Acta* **2017,** *258*, 1053-1058.

202. Largeot, C.; Portet, C.; Chmiola, J.; Taberna, P.-L.; Gogotsi, Y.; Simon, P., Relation between the Ion Size and Pore Size for an Electric Double-Layer Capacitor. *J Am Chem Soc* **2008,** *130* (9), 2730-2731.

203. Khorolsuren, B.; Lu, S.; Sun, C.; Jin, F.; Mo, W.; Song, J.; Dong, K., Investigation of the Resistive Switching Mechanisms and Rectification Characteristics of HfO_2-Based Resistive Random Access Memory Devices with Different Electrode Materials. *Journal of nanoscience and nanotechnology* **2020,** *20* (10), 6489-6494.

204. Tu, Z.; Zachman, M. J.; Choudhury, S.; Wei, S.; Ma, L.; Yang, Y.; Kourkoutis, L. F.; Archer, L. A., Nanoporous Hybrid Electrolytes for High-Energy Batteries Based on Reactive Metal Anodes. *Advanced Energy Materials* **2017,** *7* (8), 1602367.

205. Wasileski, S. A.; Weaver, M. J., Electrode Potential-Dependent Anion Chemisorption and Surface Bond Polarization As Assessed by Density Functional Theory. *The Journal of Physical Chemistry B* **2002,** *106* (18), 4782-4788.

206. Gharpure, P.; Veeralingam, S.; Badhulika, S., Bio-inspired uniform flow microfluidic sensor platform for multi-analyte sensing: a simulation-based outflow and injection study. *Microfluidics and Nanofluidics* **2021,** *25* (10), 84.

207. da Silva, G. C.; de Assis, F. S.; Monteiro, S. N.; Candido, V. S.; Rios da Silva, A. C., Evaluation of Temperature Influence on Tensile Strength and Izod Impact Resistance on Poly Methyl Methacrylate (PMMA). *Materials Science Forum* **2020,** *1012*, 100-105.

208. Deste, G.; Durkan, R.; Oyar, P., THE EFFECT OF AUTOCLAVE POLYMERIZATION ON THE TENSILE STRENGTH OF VARIOUS DENTURE BASE MATERIALS. *Cumhuriyet Dental Journal* **2020,** *23* (4), 364-370.

209. Adibeig, M. R.; Hassanifard, S.; Vakili-Tahami, F.; Hattel, J. H., Experimental investigation of tensile strength of friction stir welded butt joints on PMMA. *Materials Today Communications* **2018,** *17*, 238-245.

210. Zidan S, S. N., Haider J, Alhotan A, Jahantigh J, Yates J. , Assessing Tensile Bond Strength Between Denture Teeth and Nano-Zirconia Impregnated PMMA Denture Base. . *Int J Nanomedicine.* **2020,** *15*, 9611-9625.

211. Kihal, N.; Côté-Cyr, M.; Nazemi, A.; Bourgault, S., Semiconductive and Biocompatible Nanofibrils from the Self-Assembly of Amyloid π-Conjugated Peptides. *Biomacromolecules* **2023,** *24* (3), 1417-1431.

212. Sreekantha Reddy, S.; Yammani, C., Parameter extraction of single-diode photovoltaic module using experimental current–voltage data. **2022,** *50* (2), 753-771.

213. Machnev, A.; Ofer, D.; Shishkin, I.; Kozlov, V.; Diaferia, C.; Accardo, A.; Morelli, G.; Apter, B.; Inberg, A.; Rosenman, G.; Ginzburg, P., Amplified spontaneous emission

and gain in highly concentrated Rhodamine-doped peptide derivative. *Sci Rep* **2021,** *11* (1), 17609.

214. Wang, B.; Gao, Y.; Li, H. W.; Hu, Z. P.; Wu, Y., The switch-on luminescence sensing of histidine-rich proteins in solution: a further application of a Cu2+ ligand. *Org Biomol Chem* **2011,** *9* (11), 4032-4.

215. Kazmi, N. S.; Yan, R.; Viumdal, H.; Mylvaganam, S. J. L. E. C. P., Multimodal sensor suite for identification of flow regimes and estimation of phase fractions and velocities – Machine Learning Algorithms in Multiphase flow metering and Control. **2023**.

216. Deshpande, S.; Datar, R.; Pramanick, B.; Bacher, G., Machine Learning-Assisted Analysis of Electrochemical Biosensors. *IEEE Sensors Letters* **2023,** *7* (9), 1-4.

217. Zhang, J.; Srivatsa, P.; Ahmadzai, F. H.; Liu, Y.; Song, X.; Karpatne, A.; Kong, Z.; Johnson, B. N., Reduction of Biosensor False Responses and Time Delay Using Dynamic Response and Theory-Guided Machine Learning. *ACS Sensors* **2023,** *8* (11), 4079-4090.

218. Chong, J.; Wishart, D. S.; Xia, J., Using MetaboAnalyst 4.0 for Comprehensive and Integrative Metabolomics Data Analysis. **2019,** *68* (1), e86.

219. Inuiguchi, M.; Sakawa, M.; Ushiro, S. J. P. o. t. I. F. S. C., Mean-absolute-deviation-based fuzzy linear regression analysis by level sets automatic deduction from data. **1997,** *2*, 829-834 vol.2.

220. Vanier, A.; Sébille, V.; Blanchin, M.; Hardouin, J.-B., The minimal perceived change: a formal model of the responder definition according to the patient's meaning of change for patient-reported outcome data analysis and interpretation. *BMC Medical Research Methodology* **2021,** *21* (1), 128.

221. Verhaeghe, J.; Dhaese, S. A. M.; De Corte, T.; Vander Mijnsbrugge, D.; Aardema, H.; Zijlstra, J. G.; Verstraete, A. G.; Stove, V.; Colin, P.; Ongenae, F.; De Waele, J. J.; Van Hoecke, S., Development and evaluation of uncertainty quantifying machine learning models to predict piperacillin plasma concentrations in critically ill patients. *BMC medical informatics and decision making* **2022,** *22* (1), 224.

222. Ullah, R.; Khan, S.; Ali, Z.; Ali, H.; Ahmad, A.; Ahmed, I., Evaluating the performance of multilayer perceptron algorithm for tuberculosis disease Raman data. *Photodiagnosis and Photodynamic Therapy* **2022,** *39*, 102924.

223. Sharifi, A.; Alizadeh, K., A Novel Classification Method Based on Multilayer Perceptron-Artificial Neural Network Technique for Diagnosis of Chronic Kidney Disease. **2020,** *18* (1), e101585.

224. van Doorn, W.; Foreman, Y. D.; Schaper, N. C.; Savelberg, H.; Koster, A.; van der Kallen, C. J. H.; Wesselius, A.; Schram, M. T.; Henry, R. M. A.; Dagnelie, P. C.; de Galan, B. E.; Bekers, O.; Stehouwer, C. D. A.; Meex, S. J. R.; Brouwers, M., Machine learning-based glucose prediction with use of continuous glucose and physical activity monitoring data: The Maastricht Study. *PLoS One* **2021,** *16* (6), e0253125.

225. Zarei, A.; Rezaei, A.; Shahlaei, M.; Asani, Z.; Ramazani, A.; Wang, C., Selective and sensitive CQD-based sensing platform for Cu2+ detection in Wilson's disease. *Scientific Reports* **2024,** *14* (1), 13183.

226. Nishihara, R.; Kurita, R., Mix-and-read bioluminescent copper detection platform using a caged coelenterazine analogue. *Analyst* **2021,** *146* (20), 6139-6144.

227. Matsumoto, K.-i.; Makimoto, N. In *Time Series Prediction with LSTM Networks and Its Application to Equity Investment*, 2020.

228. Shen, Q.; Wu, Y.; Jiang, Y.; Zeng, W.; A. K. H, L. A. U.; Vianova, A.; Qu, H. In *Visual Interpretation of Recurrent Neural Network on Multi-dimensional Time-series Forecast*, 2020 IEEE Pacific Visualization Symposium (PacificVis), 3-5 June 2020; 2020; pp 61-70.

229. Ushaa, E.; Vishal, E.; Keerthna, M.; Vivek, E. J. i.-m. s. J. o. S. E., Machine learning for detecting substance use behaviors from wearable biosensor data streams: A survey and outlook for 5G/6G connectivity. **2023**.

230. Tian, Y.; Chao, M. A.; Kulkarni, C.; Goebel, K.; Fink, O., Real-time model calibration with deep reinforcement learning. *Mechanical Systems and Signal Processing* **2022,** *165*, 108284.

231. Zhou, Z.; Tian, D.; Yang, Y.; Cui, H.; Li, Y.; Ren, S.; Han, T.; Gao, Z., Machine learning assisted biosensing technology: An emerging powerful tool for improving the intelligence of food safety detection. *Current Research in Food Science* **2024,** *8*, 100679.

232. Rong, G.; Xu, Y.; Sawan, M., Machine Learning Techniques for Effective Pathogen Detection Based on Resonant Biosensors. *Biosensors (Basel)* **2023,** *13* (9).

233. Mondal, H. S.; Ahmed, K. A.; Birbilis, N.; Hossain, M. Z., Machine learning for detecting DNA attachment on SPR biosensor. *Scientific Reports* **2023,** *13* (1), 3742.

234. Vonnie, J. M.; Rovina, K.; Mariah, A. M. A.; Erna, K. H.; Felicia, W. X. L.; 'Aqilah, M. N. N., Trends in nanotechnology techniques for detecting heavy metals in food and contaminated water: a review. *International Journal of Environmental Science and Technology* **2023,** *20* (7), 8041-8072.

235. Ayyanu, R.; Arul, A.; Song, N.; Anand Babu Christus, A.; Li, X.; Tamilselvan, G.; Bu, Y.; Kavitha, S.; Zhang, Z.; Liu, N., Wearable sensor platforms for real-time

monitoring and early warning of metabolic disorders in humans. *Analyst* **2023,** *148* (19), 4616-4636.

236. Mayer, J.; Narr, J.; Pott, P. P., Towards non-invasive Wilson's disease progression monitoring based on corneal copper content. **2023,** *9* (1), 266-269.

237. Austin, K.; Torres, J. A.; Waters, J. D. V.; Balog, E. R. M.; Halpern, J. M.; Pantazes, R. J., An Orthogonal Workflow of Electrochemical, Computational, and Thermodynamic Methods Reveals Limitations of Using a Literature-Reported Insulin Binding Peptide in Biosensors. *ACS Omega* **2024,** *9* (37), 39219-39231.

238. Fracchiolla, N. S.; Artuso, S.; Cortelezzi, A., Biosensors in Clinical Practice: Focus on Oncohematology. **2013,** *13* (5), 6423-6447.

239. Johansson, C.; Hunt, H.; Signorelli, M.; Edfors, F.; Hober, A.; Svensson, A. S.; Tegel, H.; Forststrom, B.; Aartsma-Rus, A.; Niks, E.; Spitali, P.; Uhlén, M.; Szigyarto, C. A., Orthogonal proteomics methods warrant the development of Duchenne muscular dystrophy biomarkers. *Clinical proteomics* **2023,** *20* (1), 23.

240. Nishi, P.; Hardik, P.; Navin, J.; Vinit, M.; Niranjan, K.; Shrikalp, D.; Maitreyi, Z., Regulatory requirements for approval and Registration Procedure of Biosimilar in US and European Union (EU). *International Journal of Drug Regulatory Affairs* **2024,** *12* (1).

241. Amaral, C.; Rodrigues, A. R.; Veiga, F.; Bell, V., Biosimilar Medicines: From Development Process to Marketing Authorization by the EMA and the FDA. **2024,** *14* (17), 7529.